ERRATUM POSTED 15 MAY 2026; SEE LAST PAGE

Check for updates

VIROLOGY

Hepatitis E virus replication is maintained in proliferative cells within the intestinal crypt

Sarah Prallet[1,2], Niclas Maier[1]†, Albert Li[3]†, Cassian Afting[4]†‡, Hao-En Huang[5], Jungen Hu[1,2], Elif Toprak[1,2], Deb Purna Keya[6], Ombretta Colasanti[5], Nancy León-Janampa[7], Julien Marlet[7], Claudia Beisel[8], Carolin Mogler[9], Philip Puchas[10], Patrick Behrendt[11], Tobias Boettler[12], Eike Steinmann[13,14], Senjuti Saha[6], Vibor Laketa[15,16], Volker Lohmann[5,15], Joachim Wittbrodt[3], Carl Hermann[3], Michael T. Dill[10,17], Viet Loan Dao Thi[1,15]*

Copyright © 2026 The Authors, some rights reserved; exclusive licensee American Association for the Advancement of Science. No claim to original U.S. Government Works. Distributed under a Creative Commons Attribution NonCommercial License 4.0 (CC BY-NC).

The hepatitis E virus (HEV) is a leading cause of acute hepatitis worldwide. Although most infections are self-limiting, zoonotic genotypes can persist in immunocompromised individuals. Transmitted via the fecal-oral route, HEV has been suggested to directly infect the intestinal epithelium, a tissue with high regenerative capacity. Here, we demonstrate that HEV predominantly infects proliferative transit-amplifying and intestinal stem cells within the crypts of human pluripotent stem cell–derived intestinal organoids (hIOs). Supporting this, we detected HEV RNA in the intestinal crypts of an HEV-infected patient. We further found that HEV infection spreads through cell division and is maintained in hIOs for more than 40 days, contrasting with acute hepatitis A virus, whose infections are rapidly cleared from hIOs. Given the self-renewal ability and metabolic constraints of proliferative intestinal progenitor cells, our findings suggest that intestinal crypts could serve as reservoirs for chronic HEV infection and highlight the intestinal crypt as a primary target for viral infection in the gastrointestinal tract.

INTRODUCTION

Hepevirus hepatitis E virus (HEV) is a leading cause of acute viral hepatitis worldwide with an estimated 20 million annual infections (*1*). It is one of the five pathogenic human hepatitis viruses (hepatitis A to E) and the only hepatitis virus with animal reservoirs for infection. There are four major HEV genotypes infecting humans. Depending on the genotype, their transmission and regional distribution vary: HEV-1 and HEV-2 infect humans exclusively through contaminated water or food and cause large outbreaks in developing countries. These infections are usually self-limiting but can lead to fulminant hepatitis in pregnant women, with a high mortality rate of up to 25% (*2*). In contrast, HEV-3 and HEV-4 can infect a wide range of animals, including pigs and rabbits, and are mainly transmitted zoonotically to humans through the consumption of contaminated meat. Unlike HEV-1/2, most HEV-3/4 infections are asymptomatic but can lead to chronic infection in immunocompromised individuals. Recently, a distantly related strain of rat HEV was also found to infect and cause chronic infection in humans (*3*). It has yet to be determined whether other hepeviruses, including those from sheep or squirrels, can infect humans.

Despite increasing awareness and an apparent medical need, HEV remains chronically understudied. As a result, a direct-acting antiviral treatment for HEV infection has not yet been developed. Patients with chronic HEV are treated with off-label ribavirin (RBV) (*4*) and pegylated interferon-α. These drugs have serious side effects, and treatment failures due to resistance have been reported (*5*, *6*). Additionally, a protective vaccine is not universally available (*7*).

HEV has a positive single-stranded RNA genome of 7.2 kb, encoding three main open reading frames (ORFs) (*8*). ORF1 encodes the nonstructural proteins mediating genome replication, ORF2 encodes the capsid protein, and ORF3 encodes a small phosphoprotein involved in viral egress (*9*). HEV enters and exits the human body in its nonenveloped form (nHEV) and circulates in the blood cloaked in a host-derived lipid quasi-envelope (eHEV) acquired during virus budding from cells. This quasi-envelope shields HEV particles from neutralizing antibodies and facilitates their systemic spread within the host. The stable nHEV form is highly infectious, shed in feces, and underpins epidemic transmission (*10*).

Although the liver is recognized as HEV's primary target for infection, emerging evidence indicates that HEV can also infect the intestinal epithelium. For example, HEV RNA was found in the intestine of infected swine and rabbits (*11*–*14*). HEV antigen was further detected in the digestive tract of a chronically infected patient (*15*). Last, León-Janampa and colleagues identified several mutations in the HEV genome of chronically infected pigs that were associated with virus compartmentalization in feces and intestinal

[1]Schaller Research Group, Department of Infectious Diseases, Virology, Heidelberg University, Medical Faculty Heidelberg, Heidelberg, Germany. [2]Heidelberg Biosciences International Graduate School (HBIGS), Heidelberg, Germany. [3]Institute for Pharmacy and Molecular Biotechnology, Heidelberg University and BioQuant, Heidelberg, Germany. [4]Centre for Organismal Studies Heidelberg (COS), Heidelberg University, Germany. [5]Department of Infectious Diseases, Molecular Virology, Heidelberg University, Medical Faculty Heidelberg, Heidelberg, Germany. [6]Child Health Research Foundation, Dhaka, Bangladesh. [7]INSERM U1259 MAVIVHe, Université de Tours et CHRU de Tours, Tours, France. [8]Department of Infectious Diseases and Tropical Medicine, Heidelberg University Hospital, Heidelberg, Germany. [9]Institute of Pathology, School of Medicine and Health, Technical University Munich, Munich, Germany. [10]Department of Gastroenterology, Hepatology, Infectious Diseases and Intoxications, Heidelberg University Hospital, Heidelberg, Germany. [11]TWINCORE, Centre for Experimental and Clinical Infection Research, A Joint Venture between Helmholtz - Centre for Infection Research and Hannover Medical School, Hannover, Germany. [12]Department of Medicine II, Medical Center - University of Freiburg, Faculty of Medicine, Freiburg, Germany. [13]Department for Molecular and Medical Virology, Faculty of Medicine, Ruhr University Bochum, Bochum, Germany. [14]German Centre for Infection Research, External Partner Site, Bochum, Germany. [15]German Centre for Infection Research (DZIF), Partner Site Heidelberg, Heidelberg, Germany. [16]Department of Infectious Diseases, Virology, Heidelberg University, Medical Faculty Heidelberg, Heidelberg, Germany. [17]German Cancer Research Center (DKFZ) Heidelberg, Experimental Hepatology, Inflammation and Cancer, Heidelberg, Germany.
*Corresponding author. Email: vietloan.daothi@med.uni-heidelberg.de
†These authors contributed equally to this work.
‡Present address: German Red Cross Blood Donation Service Baden-Württemberg - Hessen, Institute for Transfusion Medicine and Immunohematology, 60528 Frankfurt am Main, Germany.

Downloaded from https://www.science.org at Deutsches Krebsforschungszentrum on June 05, 2026

ERRATUM POSTED 15 MAY 2026; SEE LAST PAGE

tissues. This finding is consistent with the possibility of extrahepatic HEV replication and adaptation to the digestive tract (*16*).

In vitro, the intestinal epithelial cell line Caco-2 supports HEV infection (*17*). HEV infection was reported to induce a type III interferon (IFN) response and was less sensitive to RBV treatment in human primary intestinal cells and polarized enterocytes (*15*). However, these in vitro models recapitulate only a fraction of the intestinal epithelium's cellular complexity and heterogeneity.

The intestinal epithelium is organized along a crypt-villus axis, enabling continuous self-renewal and functional specialization. At the base of the crypts reside leucine-rich repeat-containing G protein–coupled receptor 5 $(LGR5)^+$ intestinal stem cells (ISCs), which give rise to proliferative transit-amplifying (TA) cells. As cells migrate upward toward the villus (in the small intestine) or the luminal surface (in the colon), they differentiate into specialized lineages, including absorptive enterocytes, mucus-secreting goblet, hormone-producing enteroendocrine, and antimicrobial Paneth cells. One exception to this migratory path is the Paneth cells, which follow a downward migratory path to the crypt bottom and intermingle with ISCs (*18*). Enterocytes, the most abundant cell type in the intestine, have a short half-life of ~1 to 2 days in vivo after which they are shed at the villus tip. This dynamic turnover supports intestinal homeostasis, nutrient absorption, and barrier function (*19*, *20*).

Recently, several studies have used human intestinal organoids (hIOs) to investigate HEV infection, a model that better recapitulates key features of the human intestinal epithelium, including cellular diversity, crypt-villus architecture, and self-renewal (*21*). On the basis of electroporation-mediated delivery of HEV genomes, Liu *et al.* demonstrated HEV replication across multiple intestinal epithelial cell types in hIOs, while Santos-Ferreira *et al.* found HEV replication mainly in proliferative intestinal cells (*22*, *23*). Liu *et al.* reversed the polarity of hIOs to allow productive HEV infection of several cell types within hIOs (*24*).

Therefore, the question remains: Which intestinal cell type is targeted by authentic HEV infection, and how can the infection be maintained within a tissue that is characterized by a high turnover rate in vivo? To address these knowledge gaps, we used human pluripotent stem cell–derived hIOs. We find that hIOs are permissive for cell culture–derived HEV and HEV isolate infection. In the liver, HEV infects primarily epithelial cells, including hepatocytes and cholangiocytes (*10*, *25*). We identify highly proliferative TA cells and $LGR5^+$ ISCs within the crypts as a major target for HEV infection in hIOs and validate these findings in a patient with HEV. We further find that the infection can spread through cell division and is thereby likely maintained within the proliferative intestinal crypts. Together, these findings suggest a peculiar mechanism of viral persistence that exploits the self-renewal capacity of the intestinal tissue.

RESULTS

Human pluripotent stem cell–derived intestinal organoids are permissive for HEV infection

To study HEV infections of the human intestine, we differentiated the human induced pluripotent stem cell (iPSC) line iPSC.3A into intestinal organoids (hIOs) using a commercial three-stage protocol. At the end of the differentiation protocol, we obtained fully differentiated hIOs, as evidenced by the presence of various intestinal cell types expressing respective key marker proteins such as Villin (VIL; enterocyte cell marker), Mucin2 (MUC2; goblet cell marker), chromogranin A (CHGA; enteroendocrine cell marker), and lysozyme (LYZ; Paneth cell marker) (fig. S1, A to C). By RNA–fluorescence in situ hybridization (FISH) and immunofluorescence staining, we detected *LGR5* RNA (fig. S2, A and B) and Ki-67 (a proliferative marker of TA cells; figs. S1D and S2C), respectively, primarily in protruding crypt-like structures. These results demonstrated that hIOs recapitulated the native crypt-villus axis.

First, we infected hIOs with cell culture–derived HEV (HEVcc, HEV-3 Kernow-C1 p6 strain). In contrast to ultraviolet (UV)–treated HEV particles (dotted line), we observed an increase in HEV genomes from day 1 onward after infection with untreated HEV particles (green line), suggesting active replication (Fig. 1A). Detected genomes at the earliest time point of 6 hours postinfection corresponded to residual viral inoculum. To further confirm that the detected RNA in the infected hIOs by day 7 postinfection represented active HEV replication, we pretreated the virus inoculum with convalescent HEV patient serum containing mainly anti-ORF2 antibodies (*26*) before infecting hIOs. As shown in Fig. 1B (nonnormalized data in fig. S3A), pretreating HEVcc with the patient serum reduced the infection by up to 90%. Likewise, HEVcc infection was inhibited by up to 50 and 80% when pretreating hIOs with IFN-β1a and IFN-λ1, respectively (Fig. 1C and nonnormalized data in fig. S3B). Last, we detected ORF2-positive cells within HEVcc-infected hIOs by immunofluorescence staining (Fig. 1, D and E).

Of note, we have also infected adult colon and small intestinal stem cell (ASC)–derived organoids with HEVcc. Both types of organoids were permissive for infection and supported replication. However, HEVcc replication only increased in the small intestinal but less in the colon-derived organoids (fig. S4, A and B). In both ASC-derived organoid types, HEV replication levels remained lower than those observed in iPSC-derived hIOs, which is why we proceeded with iPSC-derived hIOs for the rest of our study.

We and others have previously demonstrated that nHEV particles are released apically and eHEV particles are released basally from polarized hepatocytes (*27*). nHEV particles can be further harvested from lysates recovered from HEV-infected cells (*27*). To investigate whether hIOs can recapitulate the entire HEV life cycle, we collected apical and basal cell culture supernatants, as well as cell lysates, from HEVcc-infected hIOs. Potential progeny virus was titrated on hepatoma HepG2/C3A cells, which are highly permissive for HEV infection (*8*). As shown in Fig. 1F and fig. S5 (A to C), infectious progenies were released in the apical supernatant and cell lysates, but not in the basal supernatant. Pretreatment with the convalescent patient serum strongly reduced the infection by progenies harvested from cell lysates. However, progenies released into apical supernatants were less sensitive to the treatment (Fig. 1F), suggesting the release of partially enveloped particles from the apical membrane of HEVcc-infected hIOs.

Next, we investigated whether hIOs could also be infected with primary, non–cell culture–adapted HEV. To this end, we isolated viruses from the stool of HEV-infected patients. As shown in Fig. 1G, hIOs were permissive to infection by both HEV-1 and HEV-3 isolates, although viral replication occurred at lower levels than with HEVcc. Next, we isolated HEV-3f from the stool of a chronically infected pig, containing viral species with mutations, such as the Y590C in ORF1. These mutations were present only in the virus isolated from the intestinal compartment and in the feces, but not in liver or serum (*16*). Upon infection with the same amount of genome equivalents (GEs), this isolate replicated to higher levels in hIOs than the

Downloaded from https://www.science.org at Deutsches Krebsforschungszentrum on June 05, 2026

ERRATUM POSTED 15 MAY 2026; SEE LAST PAGE

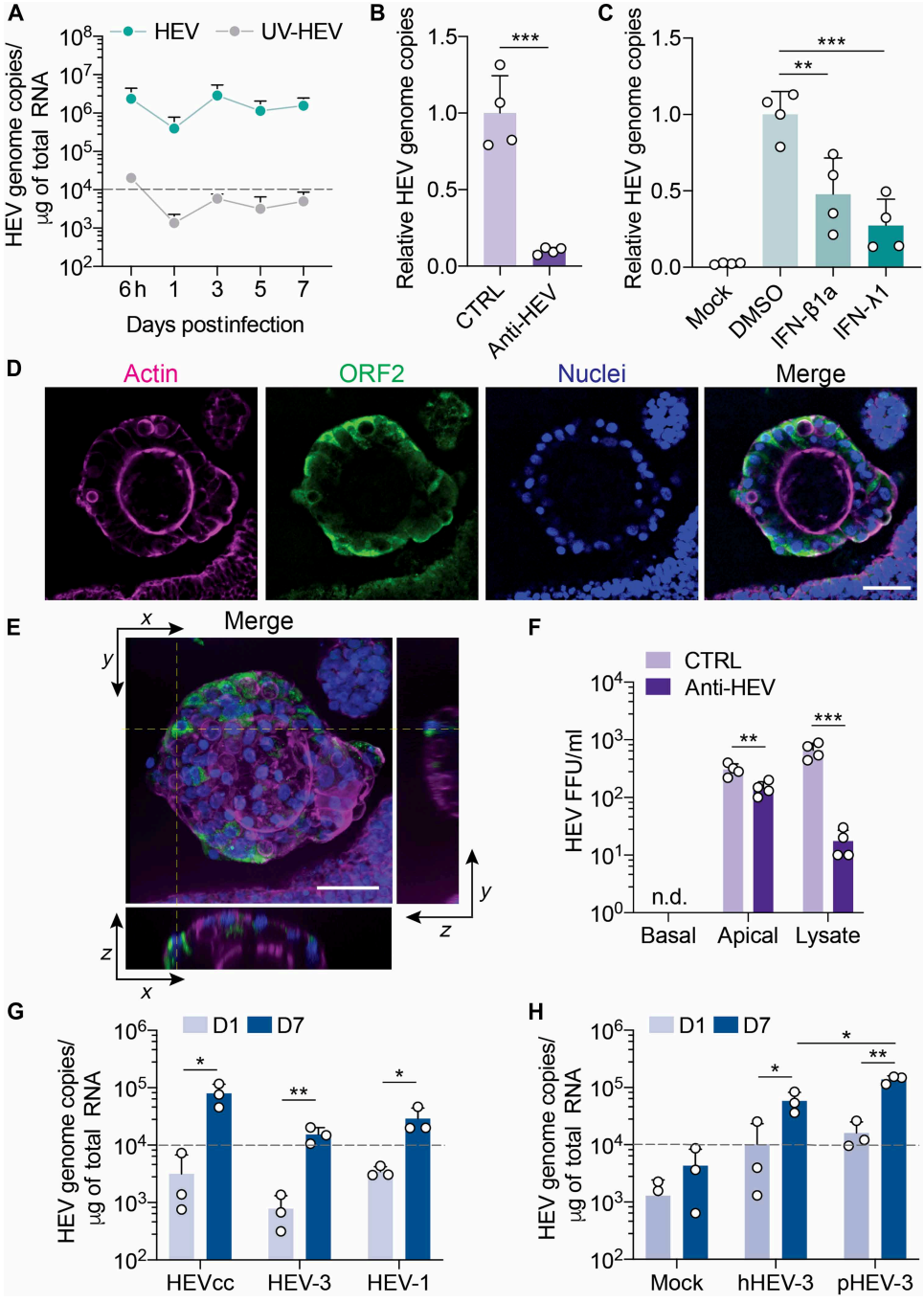


Fig. 1. Human pluripotent stem cell–derived intestinal organoids are permissive for HEV infection. (**A**) hIOs were infected with UV-treated or untreated HEV-3 Kernow-C1 p6 (HEVcc) [multiplicity of infection (MOI) of 1×10^6 genome equivalents (GEs) per well]. GEs were quantified at indicated day postinfection (p.i.). $n = 4$ biological replicates from two independent experiments. h, hours. (**B**) HEVcc was pretreated with convalescent patient (anti-HEV) or control (CTRL) serum before infection of hIOs. GEs were quantified 7 days p.i. $n = 4$ biological replicates from two independent experiments. (**C**) hIOs were pretreated with IFN-β1a (500 IU/ml) or IFN-λ1 (100 ng/ml) 24 hours before HEVcc infection and replenished every 2 days. GEs were quantified 7 days p.i. $n = 4$ biological replicates from two independent experiments. Mock, uninfected. (**D**) hIOs were infected with HEVcc (MOI of 7×10^6 GEs per well) and stained for ORF2 (green), actin (magenta), and nuclei (blue). Scale bar, 50 µm. (**E**) Three-dimensional projection of (D) and orthogonal views created with ImageJ. Scale bar, 50 µm. (**F**) HEV progenies from intracellular, basal, and apical hIO-fractions were preincubated with anti-HEV or CTRL serum for 1 hour at 37°C before infecting HepG2/C3A cells. Seven days p.i., cells were stained focus-forming units (FFUs) were counted manually. $n = 4$ replicates. n.d., not detected. (**G**) hIOs were infected with HEVcc, HEV-1, or HEV-3 isolates (MOI of 1×10^6 GEs per well), and GEs were quantified day 7 p.i. $n = 3$ biological replicates from three independent experiments. (**H**) hIOs were infected with human HEV-3f isolate and swine HEV-3f Y590H isolate (MOI of 5×10^6 GEs per well), and GEs were quantified 7 days p.i. $n = 3$ biological replicates from three independent experiments. D, day. Statistical analysis was performed by multiple comparisons of unpaired two-tailed Student's test. $^*P < 0.05$; $^{**}P < 0.01$; $^{***}P < 0.001$. Dashed line, limit of quantification (LOQ).

Downloaded from https://www.science.org at Deutsches Krebsforschungszentrum on June 05, 2026

ERRATUM POSTED 15 MAY 2026; SEE LAST PAGE

original human HEV-3f isolate, which was used to infect the pigs (Fig. 1H). This result further supported adaptation of HEV genomes to the intestinal compartment.

HEV, but not HAV, infection is maintained within hIOs

HEV-3 can lead to chronic infection in immunocompromised patients. This stands in contrast to hepatitis A virus (HAV), an enterically transmitted hepatotropic virus that almost exclusively leads to acute, self-limiting infection (*28*). Thus, we sought to compare the infection of hIOs by HEV-3 with infection of hIOs by HAV.

First, we confirmed that hIOs are also permissive for HAV infection using an HAV genotype IIIa isolate. HAV genomes increased and replicated over time postinfection (pink line), while UV-treated HAV did not (dotted line) (Fig. 2A). As observed for HEV, the HAV genomes detected at 3 hours postinfection likely represented viral RNA from the inoculum rather than products of active replication. To validate productive infection, we observed inhibition of HAV replication when hIOs were pretreated with IFNs (Fig. 2B, nonnormalized data in fig. S3C). We also detected HAV VP3 antigen-positive cells by immunofluorescence staining (Fig. 2C). Of note, while HEV infection of dissociated organoids led to productive infection, HAV infection was more successful when the particles were delivered via microinjection directly into the hIOs, as evidenced by an increase of HAV genomes over time (fig. S6, A and B). The dissociation of hIOs likely triggers a regenerative response (*29*, *30*). In agreement, we observed an enhanced expression of progenitor markers, including *LGR5*, *OLFM4*, and *SOX9*, shortly after dissociation, but not upon microinjection (fig. S7, A to D).

We then infected hIOs with either HAV or HEV and passaged them four times over a period of 50 days postinfection. HAV replication in infected hIOs declined rapidly after 4 days to undetectable levels at day 20 postinfection (Fig. 2D). In contrast, HEV replication was maintained in infected hIOs for more than 40 days postinfection (Fig. 2E). By this time point, hIOs had exhausted their proliferative capacity and began to lose epithelial integrity.

Downloaded from https://www.science.org at Deutsches Krebsforschungszentrum on June 05, 2026

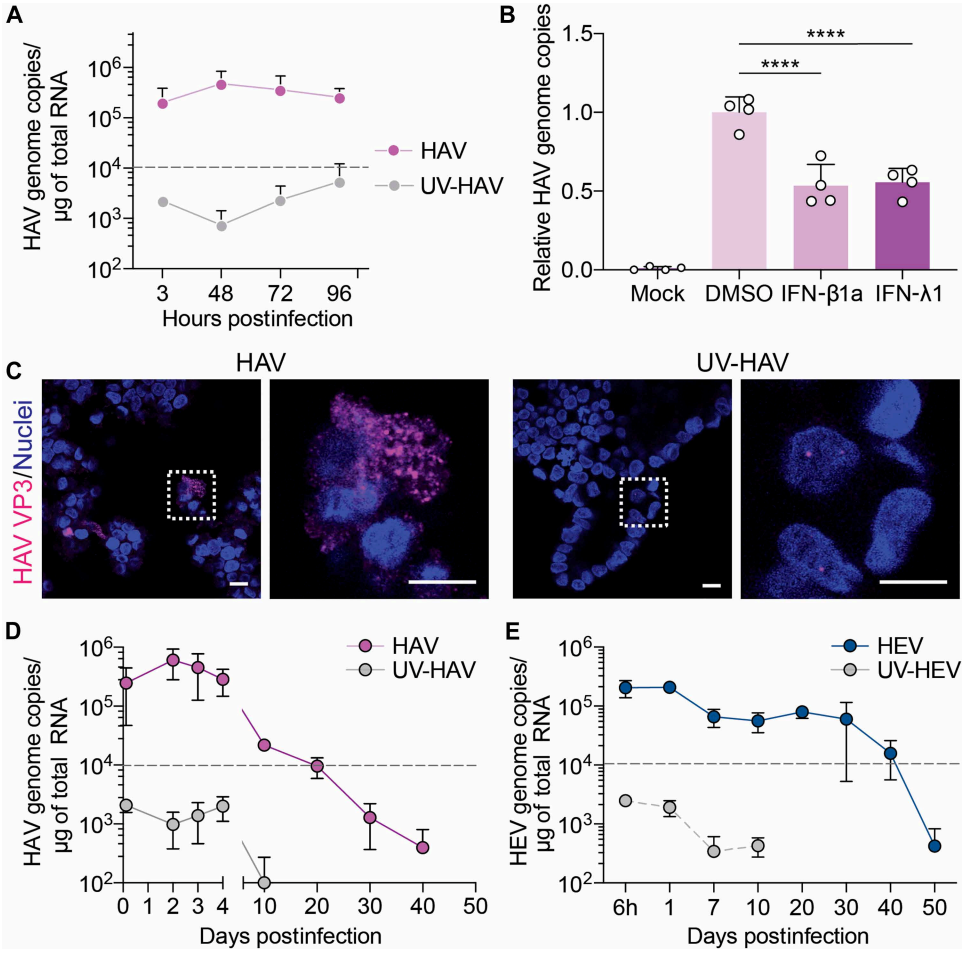


Fig. 2. HEV, but not HAV, infection is maintained within hIOs. (**A** and **B**) hIOs were infected with UV-treated or untreated HAV GTIII isolate (3×10^6 GEs per well) and (A) HAV GEs were quantified over time post infection. (B) hIOs were treated with IFN-β1a (500 UI/ml) or IFN-λ1 (100 ng/ml) 24 hours prior HAV infection and replenished every 2 days. HAV GEs were quantified at 4 days p.i. $n = 3$ independent biological experiments. (**C**) hIOs were stained for HAV VP3 protein (magenta) at 4 days p.i. Nuclei were stained with Hoechst (blue). Scale bars, 10 µm. DMSO, dimethyl sulfoxide. (**D**) hIOs were infected with either HAV (3×10^6 GEs per well) or (**E**) HEVcc (1×10^6 GEs per well) with or without UV treatment, and infected hIOs were passaged four times over a period of 50 days. Viral RNA was quantified over time at indicated time points. Results represent the means ± SD of $n = 3$ biological replicates from two independent experiments. Statistical analysis was performed by multiple comparisons of ordinary one-way analysis of variance (ANOVA). ****$P < 0.0001$. Dashed line, LOQ.

ERRATUM POSTED 15 MAY 2026; SEE LAST PAGE

HEV infects proliferative cells in the intestinal crypts of hIOs

The intestinal epithelium is a dynamic and multifaceted tissue composed of diverse cell types that perform various functions. Enteric viruses, such as rotavirus, astrovirus, and HAV, have been shown to rapidly reach a replication plateau within the first 24 hours after infecting intestinal epithelial Caco-2 cells (*31*, *32*). In contrast, HEV requires ~5 days to reach its replication plateau in Caco-2 cells (fig. S8) (*33*). Because epithelial cells are rapidly replaced in the intestine, this observation raised the possibility that HEV infects a different cell type within hIOs. To identify the specific cell types, we analyzed HEVcc-infected hIOs at 14 days postinfection by single-cell RNA sequencing (scRNA-seq) analysis using microfluidics-based 3′-targeted 10x Genomics and Illumina sequencing.

After applying quality control, a total of 17,902 single cells were used for downstream analysis (fig. S9, A and B). Based on the expression of established marker genes, cells were annotated into major intestinal cell types using a custom reference (table S1), including ISCs, enterocytes, TA, goblet, enteroendocrine, and Paneth cells (Fig. 3, A and B, and fig. S9C).

The expression of selected marker genes for each cell on Uniform Manifold Approximation and Projection (UMAP) is shown in fig. S10 (A to F). To further validate these cell-type assignments, we performed stemness scoring inference and a pseudotime trajectory analysis (fig. S11, A to C). This analysis revealed that TA cells and ISCs exhibited higher stemness scores, while differentiated cell types (e.g., enterocytes and goblet cells) showed lower scores, consistent with their mature phenotypes (fig. S11, A and B). The resulting pseudotime ordering recapitulated the expected differentiation hierarchy and demonstrated the presence of a continuous differentiation spectrum from ISCs to mature lineages in our hIOs (fig. S11C).

To identify HEV-infected cells, we quantified the presence of viral transcripts (*ORF1* or *ORF2*) at the single-cell level. A total of 500 cells showed detectable HEV RNA, yielding an overall infection rate of 2.78%. Infected cells were not randomly distributed across the intestinal cell types (Fig. 3C). Notably, TA cells, ISCs, and enterocytes represented the most abundant cell type among infected cells (Fig. 3D). We also detected HEV transcripts in Paneth, goblet, and enteroendocrine cells, but only to a smaller extent (Fig. 3D and table S2). When assessing host responses to HEV infection across the different cell types, we found that only enterocytes exhibited an up-regulation of IFN-stimulated genes [ISGs; based on (*34*)] in response to HEV infection (Fig. 3E and fig. S12).

To validate the cellular tropism of HEV in hIOs, we performed immunofluorescence staining. Both Ki-67 and KLF5 are proteins highly expressed in proliferating cells, such as TA cells (*35*–*37*). We confirmed HEV infection of TA cells in both iPSC- and ASC-derived hIOs (figs. S4C and S13) by detecting HEV ORF2 in Ki-67–positive cells. Due to antibody species incompatibility, Ki-67 staining could not be performed in HAV-infected samples, and, as a surrogate, we stained for KLF5. As shown in fig. S14, no HAV VP3-positive cells were detected among KLF5-expressing cells, indicating a distinct cellular tropism of HAV within hIOs (fig. S14).

Because progenitor cell types typically express low levels of drug metabolizing enzymes (*38*), we sought to evaluate the potency of nucleoside analogs, which are given to patients with chronic HEV in the clinic. RBV, which efficiently suppressed HEVcc replication in Caco-2 cells (fig. S8), showed no significant effect on HEVcc replication in hIOs (Fig. 3F). Similarly, the potency of sofosbuvir (SOF) appeared ineffective, even at a dose 50 times the median inhibitory concentration (Fig. 3F, nonnormalized data in fig. S3D) (*39*). Notably, only direct delivery via transfection of RBV triphosphate, but not of the prodrug, led to significant inhibition of HEV replication in hIOs. This further supported the observation that HEV preferentially infects progenitors rather than fully differentiated cells (Fig. 3G and fig. S3E).

HEV infects cells in the intestinal crypts in vivo

Next, we aimed to confirm our observation that HEV infects the intestinal crypt in vivo. To this end, we analyzed tissue sections from the cecum of a patient with acute HEV infection and a control patient without HEV infection using RNA-FISH.

Using specific probes against the HEV genome (*27*) and against *LGR5* mRNA, we detected both types of RNAs in the crypts of the HEV patient's intestine, but not in the crypts of the control patient's intestine (Fig. 4A).

We also stained these sections with an antibody against OLFM4, a previously reported intestinal crypt marker (*40*). Accordingly, we also detected HEV genomes in OLFM4-positive cells within the crypts of the patient with HEV, but not in the control patient (Fig. 4B). Outside the crypts of the patient with HEV, we could not detect HEV RNA or OLFM4 (Fig. 4C).

HEV infection can spread through cell division

To better understand how HEV infection can be maintained in proliferative intestinal cells, we took advantage of a full-length HEVcc ORF2::GFP11 reporter virus that we previously developed (*41*). It is based on the insertion of a small GFP-11 tag at the C terminus of the ORF2 capsid protein by duplicating the 3′ of the HEV genome. Upon infection, cells ectopically expressing the GFP1-10 fragment become visibly fluorescent.

As shown in Fig. 5A, HEVcc ORF2::GFP11-infected S10-3 GFP1-10 cells became GFP^+ 48 hours postinfection. Live-cell microscopy revealed that infectious HEV genomes were segregated into daughter cells during cell division, resulting in new GFP^+ cells (Fig. 5A, fig. S15, and movie S1). In contrast, when S10-3 cells were cultured under low-serum conditions (1% fetal bovine serum), which are known to arrest proliferation (*42*), HEV genomes were no longer passed to neighboring cells (fig. S16 and movie S2). We also conducted similar experiments using the intestinal cell line Caco-2 expressing GFP1-10 and discovered that HEV infection can spread through cell division (fig. S17 and movie S3). These observations suggested that HEV cell division–mediated spread is likely to be tissue-independent.

HEV infection is maintained and enriched in the crypts of hIOs over time

Because HEV primarily infects proliferative TA cells and ISCs and can propagate through cell division, we aimed to study the distribution of HEVcc infection in hIOs over time. To this end, we used an LGR5 antibody and adapted a previously developed protocol to isolate $LGR5^+$ intestinal cells from patients to initiate organoid formation (*43*). By coupling the LGR5 antibody to agarose beads, we isolated $LGR5^+$ cells from HEVcc-infected hIOs on days 10, 20, or 30 postinfection (Fig. 5B).

We first analyzed the efficiency of our isolation protocol by quantifying selected gene marker expression in $LGR5^+$ and $LGR5^-$ cell fractions from HEVcc-infected hIOs at day 20 postinfection. Markers of intestinal enterocytes at the villus such as apolipoproteins *APOA1*, *APOA4*, and *APOC3* (*44*) were higher expressed in the

Downloaded from https://www.science.org at Deutsches Krebsforschungszentrum on June 05, 2026

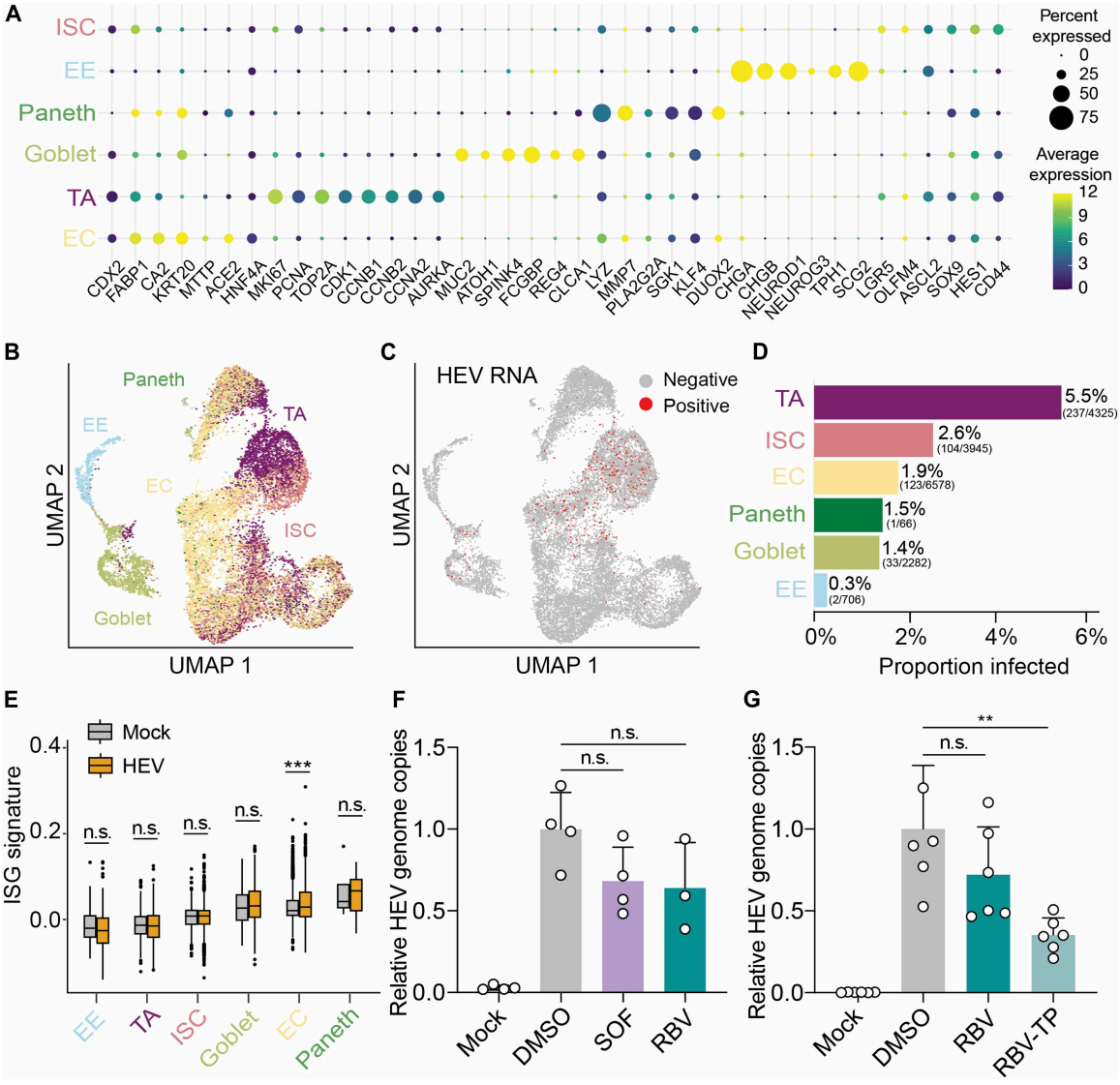


Fig. 3. scRNA-seq analysis reveals HEV infection of TA cells and ISCs in the intestinal crypts of hIOs. (**A**) Dot plot showing selected marker gene expression across cell types. Dot size represents the percentage of cells expressing each gene and dot color the average normalized expression level. (**B**) UMAP projection of 17,902 single cells pooled from two HEVcc-infected hIOs (6×10^6 GEs per well) samples at 14 days p.i., processed using microfluidics-based 3′-targeted 10x Genomics. Colors indicate distinct cell types identified through marker gene expression using SingleR, including TA cells (purple), enterocytes (EC; yellow), ISC (pink), enteroendocrine cells (EE; light blue), Goblet cells (light green), and Paneth cells (green). (**C**) HEV-infected cells identified by detection of *ORF1* and *ORF2* are highlighted in red on the UMAP ($n = 500$ infected cells). (**D**) Cell-type proportion in HEVcc-infected hIOs. (**E**) ISG signature score based on (*34*) was calculated using the AddModuleScore function in Seurat and compared between different cell types in HEV-infected hIOs (HEV-1). Statistical significance was assessed using the Wilcoxon rank sum test (one-sided, alternative = "less"), followed by Bonferroni correction for multiple testing. (**F**) hIOs were infected with HEVcc (7×10^6 GEs per well) and incubated with or without 50 μM sofosbuvir (SOF) or 100 μM RBV. Drugs were replenished every 2 days, and HEV GEs were quantified at 7 days p.i. $n = 4$ biological replicates from two independent experiments. Mock, uninfected. (**G**) hIOs were infected with HEVcc (7×10^6 GEs per well) and transfected with 100 μM RBV or RBV-triphosphate (RBV). HEV GEs were quantified 7 days p.i. $n = 6$ biological replicates from two independent experiments. Mock, uninfected. Statistical analysis was performed by multiple comparisons of ordinary one-way ANOVA. $^{**}P < 0.01$; $^{***}P < 0.001$; n.s., not significant.

LGR5$^-$ than in the LGR5$^+$ cell fraction (Fig. 5C). In contrast, we found that the stem cell marker *LGR5* and the intestinal crypt markers *SOX9* (*45*) and *OLFM4* were higher expressed in the LGR5$^+$ cell fraction than in the LGR5$^-$ cell fraction (Fig. 5D). General intestinal markers expressed in both crypt- and villus-resident cells (*MUC2*, *CDX2*, and *VIL1*) were similarly expressed in both cell fractions (Fig. 5E). Overall, these results showed that we successfully separated the crypts from the other cell types within the hIOs.

Next, we quantified the number of HEV genome copies in the LGR5$^{+/-}$ cell fractions from HEVcc-infected hIOs over time. As shown in Fig. 5F, we consistently detected a higher number of HEV genomes in the LGR5$^+$ cell fraction compared to the LGR5$^-$ cell fraction. We found ~4-fold more HEV genomes in the LGR5$^+$ cell fraction than the LGR5$^-$ fraction at 10 days postinfection, which increased to a ~10-fold difference at 30 days postinfection. Together, these results showed that HEV replication is maintained within the

Downloaded from https://www.science.org at Deutsches Krebsforschungszentrum on June 05, 2026

ERRATUM POSTED 15 MAY 2026; SEE LAST PAGE

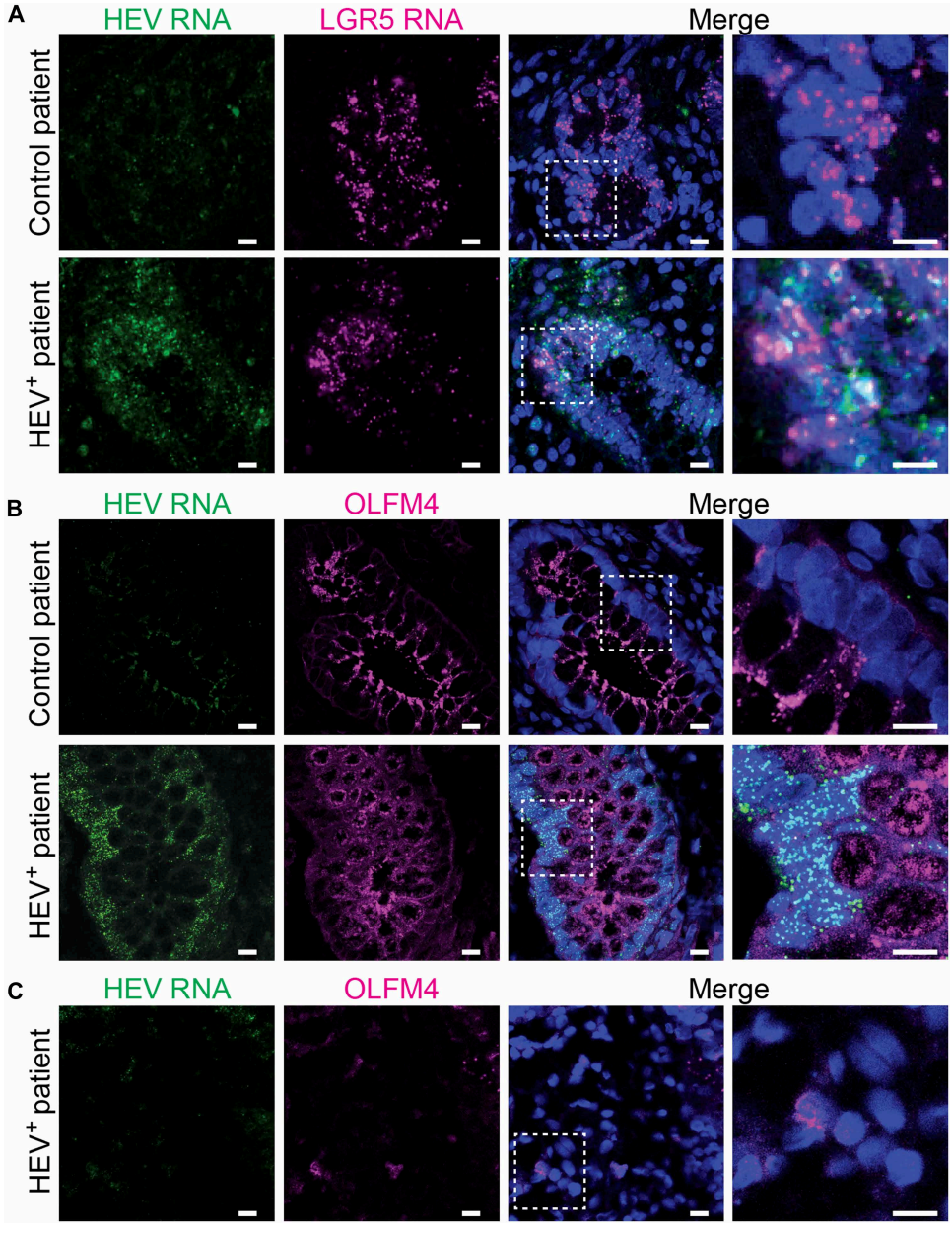


Fig. 4. HEV infects cells in the intestinal crypts of a patient. Human cecum intestinal formalin-fixed paraffin-embedded tissue sections from a patient with HEV and an uninfected control patient were analyzed by RNA-FISH to detect HEV genomes (green) and (**A**) stem cell marker *LGR5* (magenta). These tissues were further stained against in (**B**) crypt areas and in (**C**) noncrypt areas with crypt marker OLFM4 protein (magenta). Nuclei were stained with Hoechst (blue). Scale bars, 10 μm.

intestinal crypts of hIOs. Of note, marker gene expression in $LGR5^+$ and $LGR5^-$ fractions remained stable in infected hIOs (fig. S18), indicating that HEV infection did not alter cell identities over time.

DISCUSSION

HEV is transmitted via the fecal-oral route. However, the gut's role as an active viral replication site has been neglected so far. In this study, we used hIOs, which have proven to be transformative in studying other challenging enteric viruses, to demonstrate that they support infection by both HAV and HEV. Unlike HAV, HEV infection is prolonged in intestinal organoids by targeting proliferative cells within the self-renewing crypt.

The gut as an active replication site in patients with HAV and HEV

Although both HAV and HEV are recognized as enterically transmitted viruses, their direct infection of the gastrointestinal tract has remained elusive, largely due to the lack of suitable culture models. While liver-related symptoms are prominent in HAV and HEV

Downloaded from https://www.science.org at Deutsches Krebsforschungszentrum on June 05, 2026

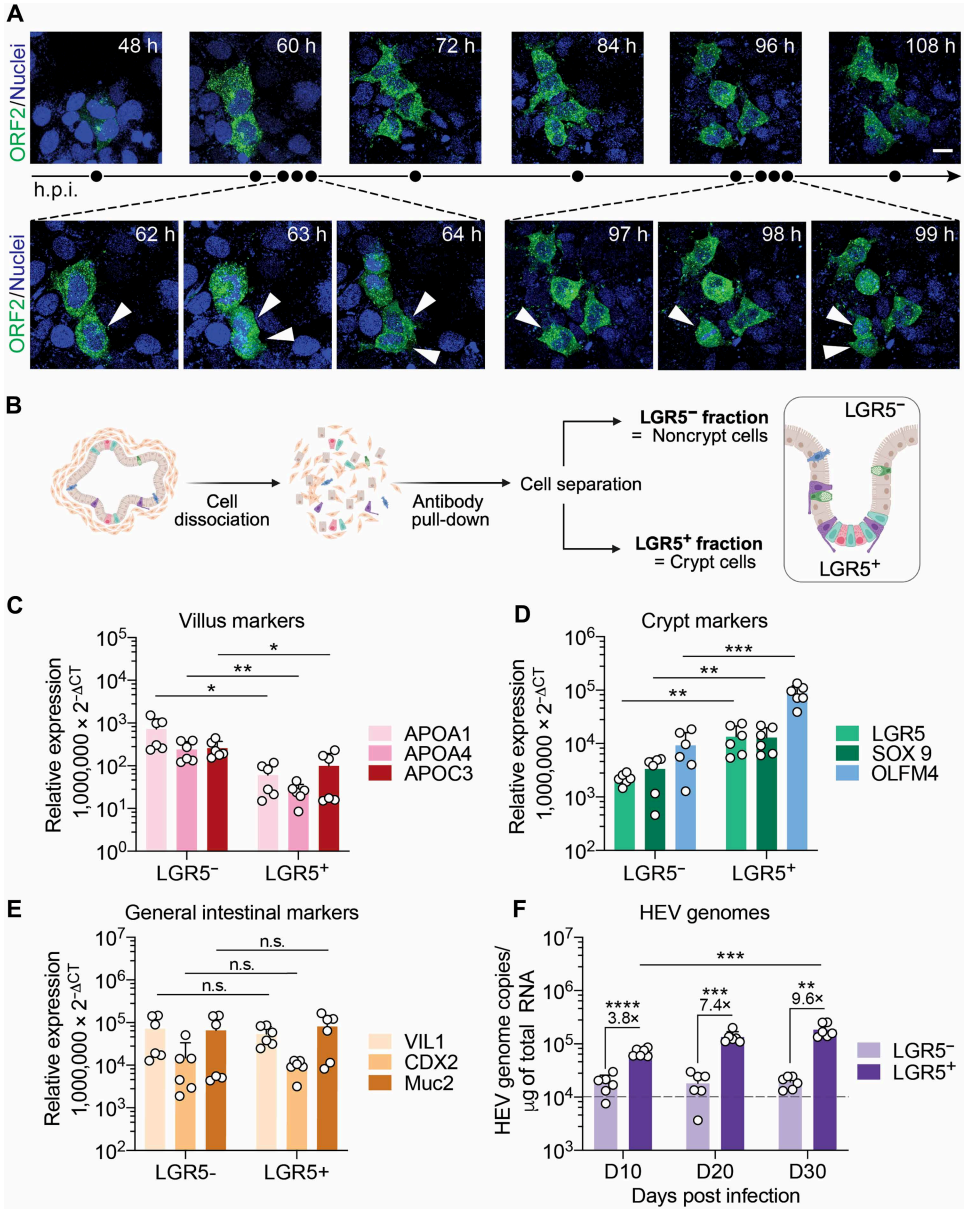


Fig. 5. HEV infection spreads through cell-to-cell division and is maintained in the crypts of hIOs. (**A**) Maximum projections of S10-3 GFP1-10 cells infected with HEV-3 cc ORF2::GFP11 and monitored by live microscopy. White arrowheads indicate dividing cells. Nuclei were stained with Hoechst (blue). h, hours; h.p.i., hours postinfection. All images are shown in fig. S15 and movie S1. Scale bar, 20 µm. (**B**) Schematic of hIOs dissociation followed by separation of LGR5$^+$ and LGR5$^-$ cells. Created in BioRender. Dao Thi, V. (2025). https://BioRender.com/5r7hvk5. (**C**) Top villus, (**D**) stem cell niche and (**E**) general intestinal marker gene expression was quantified in LGR5$^+$ and LGR5$^-$ fractions of HEVcc-infected hIOs (7×10^6 GEs per well) at 20 days p.i. ΔCycle Threshold (CT) = CT(target gene)−CT(reference gene). (**F**) HEV GEs were quantified in LGR5$^+$ and LGR5$^-$ fractions of HEVcc-infected hIOs (7×10^6 GEs per well) over time p.i. $n = 6$ biological replicates from two independent experiments. Data in (B), (C), and (D) have been assessed from the cell isolation performed on infected hIOs at D20 p.i. Statistical analysis was performed for (C), (D), and (E) by unpaired two-tailed Student's *t* test and for (F) by multiple comparisons of two-way ANOVA. *$P < 0.05$; **$P < 0.01$; ***$P < 0.001$; ****$P < 0.0001$; n.s., not significant. Dashed line, LOQ.

infections, many patients also experience gastrointestinal symptoms, including diarrhea and stomach pain, which could result directly from viral replication within the gastrointestinal tract (*46*).

Our finding that hIOs, an authentic model of the human gut epithelium, are permissive to both HAV and HEV infection supports the possibility of direct intestinal infection in vivo. Consistent with this, three very recent studies have also used intestinal organoids to highlight the critical role of the gut in HEV transmission (*22*–*24*). HEV infection of the intestine is further supported by our observation that the swine HEV-3f isolate that is specific to the intestinal tissue and feces (*16*), replicated to higher levels in hIOs than the initial human HEV-3f inoculum (Fig. 1H).

Studies using infected polarized intestinal Caco-2 cells have shown that both HAV and HEV are predominantly shed from the apical

Downloaded from https://www.science.org at Deutsches Krebsforschungszentrum on June 05, 2026

ERRATUM POSTED 15 MAY 2026; SEE LAST PAGE

surface (*17*, *47*). Marion and colleagues have described mainly apical release of HEV progenies from polarized primary small-intestine epithelial cells (*15*). In our study, we also found that HEV progeny is primarily released from the apical, but not the basal, surface of infected hIOs. Collectively, these results suggest that most of progeny viruses detected in feces may primarily originate from infected intestinal epithelial cells. This supports the hypothesis that, during acute infection, the gut, rather than the liver, may serve as the principal site of viral shedding. This hypothesis is supported by the observation of prolonged fecal shedding of viral RNA from HAV- and HEV-infected patients who underwent seroconversion (*48*, *49*).

In this scenario, infectious HEV or HAV particles can still reach the liver, for example by transcytosis or T cell–mediated cytolysis, which could lead to the release of infectious progeny into the bloodstream. Once in the liver, because it is a specialized, immune-tolerant organ (*50*), infection could be prolonged and potentially progress to chronicity, as is the case with other hepatitis viruses.

HEV primarily infects proliferative cells in the intestinal crypts enabling prolonged infection through cell division–mediated spread

While we found that both HEV and HAV can infect hIOs, only HEV infection appears to depend uniquely on self-renewal. This was first supported by the different infection routes applied. While intact organoids better supported HAV infection, the fragmentation of hIOs, which induces self-renewal as observed by the induction of *LGR5*, *SOX9*, and *OLFM4* genes, better supported HEV infection (fig. S7, A to D). The scRNA-seq analysis revealed that HEV primarily appears to infect proliferative TA cells and ISCs, rather than differentiated intestinal cell types, such as enterocytes (Fig. 3D). By analyzing isolated $LGR5^+$ fractions from infected hIOs, we further found that HEV genomes are enriched in the intestinal crypts over time. Because we used a mild dissociation method for the hIOs, we likely isolated entire crypt fragments instead of single ISCs, thus coisolating TA cells.

Most enteric and even nonenteric viruses described to date predominantly infect absorptive enterocytes rather than crypt-resident intestinal cells. For example, severe acute respiratory syndrome coronavirus 2 mainly infects enterocytes that express high levels of *ACE2* and *TMPRSS2* (*51*, *52*). Likewise, rotavirus, norovirus, and astrovirus primarily target differentiated villus cells like mature enterocytes and goblet cells in organoid models (*53*). Our discovery that HEV mainly infects crypt-resident cells represents a unique viral strategy to efficiently replicate in a tissue which is characterized by a high turnover rate in vivo. We need to acknowledge that iPSC-derived hIOs correspond to a developmentally earlier epithelial state relative to adult tissue; nevertheless, they faithfully recapitulate key architectural and cellular features of the human intestinal epithelium. Our observation is consistent with the study by Marion and colleagues (*15*), who reported the presence of HEV antigen in the crypts of a chronically infected patient. Our data further extend this observation by demonstrating that HEV replicates in ISCs, as evidenced by the detection of HEV genomes in $LGR5^+$ cells within the intestinal crypts of a patient (Fig. 4).

With an estimated half-life of 1 to 2 days, enterocytes are rather replaced rapidly and short-lived and most enteric viruses are known for their rapid replication within the host, particularly in intestinal epithelial cells. This contrasts with the slow replication dynamics of HEV infection, which takes more than 24 hours to fully establish replication (Fig. 1A and fig. S8) (*54*). Because we found that HEV infection can spread through cell division, a critical feature of HEV-permissive cells in the intestinal crypt appears to be their capacity for cell division.

Two recent HEV studies using intestinal organoids were based on electroporation-mediated delivery of HEV genomes, but not authentic infection. While Liu *et al.* (*23*) showed HEV replication in different hIOs cell types, our data are in alignment with the study by Ferreira *et al.* (*22*), who reported preferential HEV replication in proliferative TA cells. In any case, electroporation bypasses the cell entry step, which is a key determinant of viral tropism.

Cell-type–dependent innate immune responses potentially modulate HEV tropism in hIOs

In addition to taking advantage of cell proliferation and maintenance in the crypt, the cellular tropism of HEV in the intestine may also be shaped by cell-type–specific antiviral responses. Progenitor cells are characterized by a basal expression of a subset ISGs and relative refractoriness to exogenous IFN stimulation, a phenomenon that becomes attenuated as cells differentiate, rendering them more IFN-responsive (*55*). A similar cell-type–dependent response to viral infection has been reported in intestinal organoids (*51*).

In line with this maturation-dependent regulation of ISG/IFN responsiveness, we found that enterocytes mounted the strongest ISG induction upon HEV infection, whereas TA cells and ISCs showed minimal or no response. This differential responsiveness likely contributes to limiting HEV replication in enterocytes while allowing greater permissiveness in TAs or ISCs.

Although we did not observe major changes in marker gene expression of $LGR5^-$ and $LGR5^+$ fractions over time (fig. S18), we cannot fully rule out that the host response to HEV infection in hIOs leads to cell identity changes or depletion and thereby contributes to HEV persistent replication in proliferative progenitor cells. Future mechanistic studies, such as targeted knockout of IFN receptors or adaptor proteins involved in innate sensing pathways, without disrupting stemness or renewal capacity, will be therefore essential to further dissect the role of host antiviral responses in shaping HEV tropism in human intestinal organoids.

Likewise, because we observed that HEV, rather than HAV, infects intestinal progenitor cells, future studies should also investigate in how far the tissue self-renewal and/or cell-intrinsic antiviral responses contribute to the more rapid clearance of HAV infection in hIOs (Fig. 2D), potentially reflecting clinical outcomes in vivo. However, it is important to note that the connection between cell-intrinsic innate immune responses and chronic infection remains weak. Chronic HEV infection typically arises under conditions of immunosuppression, which predominantly impair adaptive immunity rather than innate antiviral defenses. Our observation that HEV, but not HAV, infects proliferative cells within hIOs indicates that the persistence of HEV infection may mainly result from its distinct cellular tropism together with its ability to spread through cell division.

HEV infection of the intestinal crypt as a potential therapeutic reservoir in chronic patients

We found that treatment with high doses of potent, HEV-inhibitory nucleoside analogs did not affect HEV replication in hIOs. However, pretreating hIOs with IFNs inhibited infection by both HEV and HAV, ruling out the possibility that small molecules fail to reach hIOs, which could otherwise explain their limited efficacy.

Downloaded from https://www.science.org at Deutsches Krebsforschungszentrum on June 05, 2026

ERRATUM POSTED 15 MAY 2026; SEE LAST PAGE

Marion *et al.* (*15*) previously demonstrated that RBV does not fully inhibit HEV release from the apical side of human polarized enterocytes in vitro. Our data further suggest that the varying metabolic states across different intestinal cell lineages may contribute to the reduced antiviral efficacy observed. Previous studies reported sensitivity of HEV replication to RBV in hIOs (*22*, *24*). However, as noted earlier, these studies introduced the viral genomes via electroporation, including into fully differentiated cell types, rather than using authentic viral infection.

In the human body, drugs are primarily metabolized by the liver and intestinal epithelial cells (*56*, *57*). Nucleoside analogs like RBV and SOF, in particular, require metabolic activation into their triphosphate forms. This process relies on enzymes that are largely absent in the intestinal crypt compartment (*58*, *59*) with key drug-metabolizing enzymes (e.g., pan-intestinal members of the CYP450 family) being nearly undetectable in crypt-domain lineages. For example, phosphorylation of RBV by adenosine kinase ADK is essential in its antiviral activity (*60*). However, scRNA-seq data show minimal *ADK* expression in TA cells and ISCs compared to abundant levels in differentiated enterocytes (*61*, *62*). This metabolic paucity within the intestinal crypt possibly explains why HEV replication is less sensitive to these antivirals in hIOs. Consequently, the limited efficacy of RBV and SOF in this compartment might facilitate the formation of a viral reservoir during treatment, potentially accounting for relapse cases as observed in patients with chronic HEV (*6*, *63*). This is further supported by our observation that only direct delivery via transfection of RBV triphosphate, but not of the prodrug, led to significant inhibition of HEV replication in hIOs (Fig. 3G).

Because we found that both acute HEV-1 and zoonotic HEV-3 can replicate in hIOs, the ability to replicate in the intestine does not appear to be a critical feature of chronic HEV infection per se. Instead, we propose that the intestinal crypt can act as a reservoir within chronic patients, which may require a drug regimen tailored to the crypt's unique metabolic profile. Critically, recent advances in culturing hIOs support large-scale drug screening efforts and have already proven valuable for cytotoxicity testing, permeability assays, and therapeutic target validation (*64*–*67*). By identifying the specific intestinal cell types infected by viruses, as demonstrated in this study, hIOs enable more precise, targeted screening strategies in the future with the overarching goal of identifying efficient and curative treatments.

MATERIALS AND METHODS

Reagents and antibodies

The following antibodies were used for immunofluorescence staining at indicated concentrations: polyclonal anti-ORF2 HEV (1:1000, a gift from R. Ulrich); anti-VP3 HAV (2 μg/ml; Invitrogen, ref. MA1-7371); anti-CDX2 (1:100; Abcam, ref. AB157524), anti-CHGA (1.75 μg/ml; Abcam, ref. AB15160); anti-Ki67 (2 μg/ml; Santa Cruz Biotechnology, ref. sc23900); anti-LYZ (1:100; Invitrogen, ref. PA1-29680); anti-MUC2 (2 μg/ml; Santa Cruz Biotechnology, ref. sc-515032); anti-VIL (0.625 μg/ml; BD, ref. 10358); anti-OLFM4 (1:100; Cell Signaling Technology, ref. 14369 T); anti-LGR5 (12.1 μg/ml; GeneTex, ref. GTX130204); and Alexa Fluor–conjugated secondary antibodies 488, 594, and 647 (2 μg/ml; Thermo Fisher Scientific). Hoechst 33342 (1:1000, Thermo Fisher Scientific) was used for nuclei staining, and Phalloidin-iFluor 647 (0.1×; Abcam, ref. AB176759) was used as a cell junction marker.

Human induced pluripotent stem cell (hiPSC)-derived intestinal organoid generation and culture

The iPSC line iPSC.3A (a gift from S. Duncan) was maintained in feeder-free conditions using mTeSR1 medium (STEMCELL Technologies) on Matrigel (Corning, ref. 354230)–coated plates as per the manufacturer's instructions. iPSC.3A cells were differentiated to small intestinal organoids using the STEMdiff Intestinal organoids Kit (STEMCELL Technologies, ref. 05140) according to the manufacturer's protocol. Organoids were grown in STEMdiff Intestinal Organoid Basal Medium (STEMCELL Technologies, ref. 05143) with 0.2% STEMdiff Intestinal Organoid Supplement (STEMCELL Technologies, ref. 05144), 0.1% L-glutamine (Gibco, ref. 25030-024). The medium was changed every 3 to 4 days.

For routine passaging every 7 to 10 days, culture medium was aspirated and replaced with ice-cold Dulbecco's modified Eagle's medium (DMEM)/F12. hIOs were released by breaking up the Matrigel domes and transferred to 15-ml conical tubes. The hIOs were mechanically fragmented using sequential pipetting with 1-ml and 200-μl pipettes until a homogeneous suspension of organoid fragments was obtained. The fragments were centrifuged at 300*g* for 5 min at 4°C, and the supernatant was carefully removed. hIOs were then reembedded in 40-μl Matrigel domes (Cultrex Reduced Growth Factor Basement Membrane Extract, ref. 3533-005-02) according to the desired splitting ratio, which was adjusted on the basis of organoid size and culture density.

HEV and HAV purification from stool samples

The HEV-3 and HAV-IIIa isolates were derived from fecal samples of patients in the gastroenterology ward of Heidelberg University Hospital during the acute phase of infection. The original HEV-3f isolate (hHEV-3) was obtained from feces of a kidney transplant patient, while the swine-passaged HEV-3f isolate (pHEV-3) was collected from feces of a chronically infected pig at week 11 postinfection (*16*). Stool samples were diluted to a 10% v/v solution with phosphate-buffered saline (PBS) and centrifuged at 1500*g* for 10 min and at 3000*g* for 30 min. The supernatant was passed through 5-μm filters (Macherey-Nagel, ref. 729242) and then centrifuged again at 3000*g* for 30 min, followed by filtering through 1.2-μm Chromafil Xtra PES filter (Macherey-Nagel, ref. 729229), 0.45-μm and 0.22-μm filter units (Millex GV, ref. SLGV033RS/004SL). UV inactivation was applied to both viruses for 30 min of UV-light exposure (UV lamp Benda, 220 V, 2 × 6 W, wavelength254 nm, N-12K).

HEV/HAV infections of hIOs and neutralization

Cell culture HEV-3 Kernow-C1/p6 strain virus was produced as previously described (*68*). For virus infections of hIOs delivered through fragmentation, culture medium was aspirated, and hIOs were harvested with 1 ml of cold DMEM/F12 per Matrigel dome and transferred into a 15-ml Falcon tube. hIOs were fragmented by pipetting them up and down at least 10 times with a P1000 and an additional 10 times with a P200. Samples were centrifuged at 300*g* for 5 min 4°C, and supernatant was carefully aspirated. hIOs recovered from one Matrigel dome were infected with 1×10^6 HEV GEs or 3.3×10^6 HAV GEs in 1 ml of STEMdiff Intestinal organoid complete medium supplemented with 10 μM Y27632 (STEMCELL Technologies, ref. 72304) and transferred into a 1.5-ml Eppendorf tube prior treated with antiadherence solution (STEMCELL Technologies, ref. 07010). Tubes were placed on an Intelli mixer rotator (neoLabLine, ref. 7-0045) in the incubator and incubated for 8 hours

Downloaded from https://www.science.org at Deutsches Krebsforschungszentrum on June 05, 2026

ERRATUM POSTED 15 MAY 2026; SEE LAST PAGE

at 10 rpm rotation at 37°C and 5% CO_2. Afterward, cells were transferred into a 15-ml Falcon tube with 5-ml PBS and centrifuged at 300*g* for 5 min. The inoculum was removed and washed three times with PBS, and hIOs were reembedded into 100% gelated Matrigel. For neutralization, HEV particles were treated with convalescent patient serum or HEV-negative patient serum at 1:1000 for 1 hour at 37°C before infecting hIOs and harvested at respective time points.

For virus infections delivered through microinjection, hIOs were grown in Matrigel domes on 12-mm glass round coverslips. The Matrigel domes were transferred onto 70% ethanol rinsed Parafilm on a plastic dish (Thermo Fisher Scientific, ref. 13-374-10), covered with gentamicin (50 μg/ml; Sigma-Aldrich, ref. G1272) containing culture medium, and injected at room temperature (RT) with borosilicate micropipettes pulled into microinjection needles with a slender taper. Microinjection needles (1-mm outer diameter by 0.58-mm inside diameter by 100-mm length; Warner Instruments, ref. 30-0016) were pulled on a Flaming/Brown micropipette puller P-97 (Sutter Instruments) using the following parameters: heat 505, pull 25, velocity 250, time 10, and 1 cycle. Needles were cut open manually with beveled openings of ~5 μm or less. Microinjections were performed with a homemade oil microinjector and a standard manual micromanipulator under an epifluorescence stereomicroscope SMZ1500 (Nikon GmbH).

HEV (1.10^6 genome copies) and HAV (1.10^7 genome copies) virus solutions were thawed on ice and mixed at a 4:1 ratio with 85 mM fluorescein (Sigma-Aldrich, ref. 46960-100G-F) to allow visualization during the procedure. For each condition, 30 to 40 hIOs per Matrigel dome were microinjected filling their lumens completely. Because hIOs within a single Matrigel dome varied in morphology and lumen volume, the injected volume differed among samples (up to 5 to 10 nl per hIO). hIOs selected for microinjection were chosen to be as uniform in morphology and size as possible. After microinjection, hIO domes were transferred back into a 24-well plate and incubated at 37°C and 5% CO_2 control until harvesting at later time points for analysis.

hIOs transfection

hIOs were processed following as for infection by fragmentation. Lipofectamine 3000 transfection reagent (1 μl; Life Technologies, ref. L3000008) was diluted in Opti-MEM (Life Technologies), and, in a separate tube, RBV or RBV-TP was diluted in Opti-MEM. The two solutions were gently combined, incubated for 15 min at RT, and added to fragmented hIOs for 6 hours at 37°C, 5% CO_2. Afterward, cells were transferred into a 15-ml conical tube containing 5 ml of PBS and centrifuged at 300*g* for 5 min. The hIOs were reembedded in 100% Matrigel and maintained in complete organoid culture medium.

LGR5$^+$ cell isolation of hIOs

Y27632 ROCK-inhibitor (10 μM) was added to hIOs at least 2.5 hours before harvest and to all solutions during the entire procedure. hIOs were infected with HEV as described above and harvested at different time points by removing the Matrigel with cell recovery solution at 4°C. hIOs were incubated in Versene solution for 5 min at 37°C. hIOs were further fragmented using first a 1-ml pipettor and a 200-μl pipettor. hIOs were dissociated by treating hIOs with gentle cell dissociation reagent (STEMCELL Technologies, ref. 100-0485), supported by 10 times repeated mechanical disruption through P1000 pipetting and slow rotation (10 rpm) for 20 min at 37°C and 5% CO_2. Single-cell suspension was incubated with 1.5 mg of Protein A agarose beads (Pierce)–bound anti-LGR5 antibody at slow rotation (10 rpm) for 2 hours at 4°C, followed by centrifugal separation at 300*g*. LGR5$^+$ and LGR5$^-$ fractions were collected and lysed with TRIzol reagent (Thermo Fisher Scientific) for RNA extraction.

FISH of viral RNA

Formalin-fixed paraffin-embedded human intestinal tissue sections from the cecum of a patient with acute HEV treated at the Technical University Munich hospital were analyzed following the Advanced Cell Diagnostics (ACD) manufacturer's RNAscope Multiplex Fluorescent Reagent Kit version 2 user manual and using probes to detect *HEV ORF1* (catalog no. 579831) and *LGR5* (catalog no. 311021).

Immunofluorescence staining of hIOs

hIOs were collected in 1.5-ml tubes, coated with antiadherence solution, and fixed with 4% paraformaldehyde overnight at 4°C or for 2 hours at RT under constant rolling. hIOs were centrifuged after each step at 300*g* for 5 min at 4°C. Samples were blocked and permeabilized in PBTG [10% goat serum, 1% bovine serum albumin (BSA), and 0.1% Triton X-100 in PBS] overnight at 4°C under constant agitation before incubation with primary antibody diluted in PBTG overnight at 4°C. Alexa Fluor–conjugated secondary antibodies were used at 1:1000 diluted in PBTG for 1 hour at RT. Hoechst 33342 (1:1000, Thermo Fisher Scientific) was used for nuclei staining. Coverslips were mounted using the ProLong Glass Antifade Mountant (Thermo Fisher Scientific) and cured for at least 24 hours in the dark before imaging.

RNA extraction and RT-qPCR

Total RNA was isolated from cell lysates using the TRIzol reagent (Thermo Fisher Scientific) according to the manufacturer's protocol. HAV RNA was detected using a one-step reverse transcription quantitative polymerase chain reaction (RT-qPCR) ToughMix (Quanta Biosciences). For HEV, reverse transcription was performed using the iScript DNA Synthesis kit (Bio-Rad), and RNA was detected using iTaq Universal SYBR Green Supermix (Bio-Rad) on a CFX96 thermocycler (Bio-Rad). Viral RNA copies and relative expression data were normalized to expression against the housekeeping gene *GAPDH* or *RPS11*. The primer sequences (forward and reverse) used for qPCR are listed in table S3.

Confocal microscopy and image analysis

Microscopy imaging was performed on an inverted Zeiss LSM900 point laser scanning confocal microscope (Carl Zeiss Microscopy GmbH) equipped with the Airyscan detector, a Spinning Disc Ti2 CREST (Nikon), a Luxendo MuVi SPIM Light Sheet microscope (Bruker), and Zeiss Cell Discoverer 7 (CD7, Carl Zeiss Microscopy GmbH) in this study. Fluorescence and bright-field images were collected with a 20× air objective or 40× oil immersion objective. Time-lapse video microscopy measurements were performed on the inverted Zeiss LSM900 with an environmental control chamber, recording interval of 1 hour, and maximum intensity projection of 13.2 μm. All images were processed using either the Zeiss ZEN Blue v3.1 microscope-control software, ImageJ, and Zeiss Arivis software.

Downloaded from https://www.science.org at Deutsches Krebsforschungszentrum on June 05, 2026

ERRATUM POSTED 15 MAY 2026; SEE LAST PAGE

3′-Targeted 10x Genomics and Illumina sequencing

For each sample, three Matrigel domes were combined to obtain sufficient cells for one 10x Genomics scRNA-seq reaction. hIOs were harvested and dissociated by incubation with TrpLEX (Gibco, ref. 12604013) 37°C for 10 min and 10× pipetting with a P1000, followed by an additional incubation step for 10 min at 37°C. DMEM/F12 (STEMCELL Technologies, ref. 36254) was added to each tube and cells were spun for 5 min at 500*g*. Cells were resuspended in 0.5% BSA/PBS and passed through a 70-µm cell strainer (Carl Roth, ref. CNA0.1). Cells were counted and inspected for viability using trypan blue. Single-cell suspensions were loaded onto the 10x Chromium controller according to manufacturer's instructions of the Chromium Next GEM Single Cell 3′ Kit v3.1 (10x Genomics, ref. 1000269) with a targeted cell recovery of 10,000. Sequencing libraries were prepared according to the manufacturer's instructions. Resulting libraries were pooled and sequenced on an Illumina NextSeq2000 (high-output mode, paired-end, 100 cycles).

scRNA-seq data analysis

Raw base call (BCL) files generated from the Illumina sequencer were demultiplexed using the Cell Ranger mkfastq pipeline (v6.1.2, 10x Genomics). Gene expression matrices were generated with Cell Ranger count, aligning reads to a custom reference genome that combined the human GRCh38 (version 3.0.0, provided by 10x Genomics) and the HEV genome (GenBank, accession no. JQ679013.1). The resulting filtered gene-barcode matrices served as input for downstream analysis in Seurat.

Gene expression matrices from HEV-infected samples were obtained from the Cell Ranger outputs. These matrices were loaded into R using the Read10X function from the Seurat (v4.4) package. Each dataset was converted into a Seurat object using CreateSeuratObject with default parameters, excluding genes expressed in fewer than three cells and cells with fewer than 200 detected genes. To filter out low-quality cells and potential doublets, cells were excluded if they had fewer than 200 or more than 9000 detected genes (nFeature_RNA), more than 100,000 total Unique Molecular Identifier (UMI) counts (nCount_RNA), or more than 50% of transcripts mapping to mitochondrial genes. Mitochondrial gene fraction was calculated using PercentageFeatureSet with the pattern "^MT-". To annotate HEV-infected cells, raw UMI counts of viral genes ORF1 and ORF2 were retrieved using FetchData and summed per cell. A cell was considered infected if the total viral gene count exceeded zero.

To integrate multiple datasets (HEV-1 and HEV-2) and correct for technical variation, the merged object was split by sample origin (orig.ident) and processed with the SCTransform workflow. Each dataset was normalized independently with default SCTransform parameters. Integration features were selected using SelectIntegrationFeatures ($n = 3000$), followed by dataset preparation (PrepSCTIntegration), anchor identification (FindIntegrationAnchors), and data integration (IntegrateData) using the SCT method. The integrated dataset was reduced in dimensionality via principal components analysis (top 30 components), followed by visualization with UMAP (RunUMAP on the top 30 principal components). Clustering was performed using FindNeighbors and FindClusters at a resolution of 0.8.

For cell-type annotation, a curated marker gene table (table S3) was used to build a custom reference. Marker genes were grouped by cell type, and a binary matrix was created assigning 1 to marker genes and 0 to all others. The integrated HEV-infected dataset served as the query, and cell types were assigned using SingleR (v1.12.1) (*69*) with this reference. To evaluate whether specific cell types were disproportionately infected, the proportion of infected cells was calculated per cell type.

To further validate the cellular heterogeneity and differentiation dynamics, we performed stemness inference and pseudotime trajectory analysis. CytoTRACE2 (*70*) was applied to quantify cellular differentiation states on the basis of transcriptional diversity. Pseudotime analysis was conducted using Monocle3 (*71*), with trajectory initialization based on stem cells ranked by CytoTRACE2 scores. The top 10 stem cells with the highest stemness scores were designated as root cells for each sample subset.

Gene set signature analysis

Gene signature scores were calculated using the AddModuleScore () function in Seurat (*72*). We analyzed two gene signatures: an ISG signature based on the study by Schoggins *et al.* (*34*) and the apoptosis signature obtained from the REACTOME pathway database (*73*). To visualize and compare signature scores between HEV-infected and mock samples across different cell types, we extract signature scores along with cell-type annotations and treatment conditions from the Seurat metadata.

Statistical analyses

Graphs were produced and statistical analyses were performed using GraphPad Prism 8 software. Experimental data for RT-PCR are reported as means ± SD. In all figures where *P* values were calculated, the corresponding statistical test is listed in the figure legend. *P* values of <0.05 were considered statistically significant.

Biosafety

Experiments involving viral infections were conducted within a Biosafety Level 2 facility at Heidelberg University and were approved by the "Regierungspräsidium Tübingen."

Declaration of generative AI and AI-assisted technologies in the writing process

During the preparation of this work, the authors used DeepL Write to improve language and readability. After using this tool/service, the authors reviewed and edited the content as needed and take full responsibility for the content of the publication.

Ethics approval statement

Work with human iPSCs (S-439/2018) and use of ASC-derived colon and small intestine organoids (S-129/2022), HEV-3 isolates (S-565/2011), and HAV isolates (S-743/2023) have been approved by the Ethics Committee of the Medical Faculty of Heidelberg University. Use of human intestinal biopsy material was approved by the local ethics committee of Klinikum Rechts der Isar (518/19 S). Use of the convalescent patient serum was approved by the Ethics Committee of the Albert-Ludwigs-University Freiburg (474/14, 201/17, and 486/19), and written informed consent was obtained from all blood donors. The Institutional Review Board for collection and use of HEV-1 isolates was obtained from the Ethical Review Committee of Bangladesh Shishu Hospital and Institute (no. Admin/BSHI/2022/2057).

Supplementary Materials

The PDF file includes:

Supplementary Methods
Figs. S1 to S18
Tables S1 to S3
Legends for movies S1 to S3
References

Downloaded from https://www.science.org at Deutsches Krebsforschungszentrum on June 05, 2026

ERRATUM POSTED 15 MAY 2026; SEE LAST PAGE

Other Supplementary Material for this manuscript includes the following:
Movies S1 to S3

REFERENCES

1. D. B. Rein, G. A. Stevens, J. Theaker, J. S. Wittenborn, S. T. Wiersma, The global burden of hepatitis E virus genotypes 1 and 2 in 2005. *Hepatology* **55**, 988–997 (2012).
2. H. R. Dalton, J. Seghatchian, Hepatitis E virus: Emerging from the shadows in developed countries. *Transfus. Apher. Sci.* **55**, 271–274 (2016).
3. S. Sridhar, C. C. Y. Yip, S. Wu, J. Cai, A. J. Zhang, K. H. Leung, T. W. H. Chung, J. F. W. Chan, W. M. Chan, J. L. L. Teng, R. K. H. Au-Yeung, V. C. C. Cheng, H. Chen, S. K. P. Lau, P. C. Y. Woo, N. S. Xia, C. M. Lo, K. Y. Yuen, Rat hepatitis E virus as cause of persistent hepatitis after liver transplant. *Emerg. Infect. Dis.* **24**, 2241–2250 (2018).
4. N. Kamar, J. Izopet, S. Tripon, M. Bismuth, S. Hillaire, J. Dumortier, S. Radenne, A. Coilly, V. Garrigue, L. D'Alteroche, M. Buchler, L. Couzi, P. Lebray, S. Dharancy, A. Minello, M. Hourmant, A. M. Roque-Afonso, F. Abravanel, S. Pol, L. Rostaing, V. Mallet, Ribavirin for chronic hepatitis E virus infection in transplant recipients. *N. Engl. J. Med.* **370**, 1111–1120 (2014).
5. D. Todt, A. Gisa, A. Radonic, A. Nitsche, P. Behrendt, P. V. Suneetha, S. Pischke, B. Bremer, R. J. Brown, M. P. Manns, M. Cornberg, C. T. Bock, E. Steinmann, H. Wedemeyer, In vivo evidence for ribavirin-induced mutagenesis of the hepatitis E virus genome. *Gut* **65**, 1733–1743 (2016).
6. A. Gömer, M. Klöhn, M. Jagst, M. K. Nocke, S. Pischke, T. Horvatits, J. S. Z. Wiesch, T. Müller, S. Hardtke, M. Cornberg, H. Wedemeyer, P. Behrendt, E. Steinmann, D. Todt, Emergence of resistance-associated variants during sofosbuvir treatment in chronically infected hepatitis E patients. *Hepatology* **78**, 1882–1895 (2023).
7. J. M. Peron, H. Larrue, J. Izopet, M. Buti, The pressing need for a global HEV vaccine. *J. Hepatol.* **79**, 876–880 (2023).
8. R. M. Fu, C. C. Decker, V. L. Dao Thi, Cell culture models for hepatitis E virus. *Viruses* **11**, 608 (2019).
9. B. Wang, X. J. Meng, Structural and molecular biology of hepatitis E virus. *Comput. Struct. Biotechnol. J.* **19**, 1907–1916 (2021).
10. A. Das, E. E. Rivera-Serrano, X. Yin, C. M. Walker, Z. Feng, S. M. Lemon, Cell entry and release of quasi-enveloped human hepatitis viruses. *Nat. Rev. Microbiol.* **21**, 573–589 (2023).
11. S. Jung, D. J. Seo, D. Yeo, Z. Wang, A. Min, Z. Zhao, M. Song, I. S. Choi, J. Myoung, C. Choi, Experimental infection of hepatitis E virus induces pancreatic necroptosis in miniature pigs. *Sci. Rep.* **10**, 12022 (2020).
12. T. P. Williams, C. Kasorndorkbua, P. G. Halbur, G. Haqshenas, D. K. Guenette, T. E. Toth, X. J. Meng, Evidence of extrahepatic sites of replication of the hepatitis E virus in a swine model. *J. Clin. Microbiol.* **39**, 3040–3046 (2001).
13. J. Izopet, M. Dubois, S. Bertagnoli, S. Lhomme, S. Marchandeau, S. Boucher, N. Kamar, F. Abravanel, J. L. Guérin, Hepatitis E virus strains in rabbits and evidence of a closely related strain in humans, France. *Emerg. Infect. Dis.* **18**, 1274–1281 (2012).
14. Q. Wu, J. An, R. She, R. Shi, W. Hao, M. Soomro, X. Yuan, J. Yang, J. Wang, Detection of genotype 4 swine hepatitis E virus in systemic tissues in cross-species infected rabbits. *PLOS ONE* **12**, e0171277 (2017).
15. O. Marion, S. Lhomme, M. Nayrac, M. Dubois, M. Pucelle, M. Requena, M. Migueres, F. Abravanel, J. M. Peron, N. Carrere, B. Suc, P. Delobel, N. Kamar, J. Izopet, Hepatitis E virus replication in human intestinal cells. *Gut* **69**, 901–910 (2020).
16. N. León-Janampa, I. Caballero-Posadas, C. Barc, F. Darrouzain, A. Moreau, T. Guinoiseau, P. Gatault, I. Fleurot, M. Riou, A. Pinard, J. Pezant, C. Rossignol, C. Gaudy-Graffin, D. Brand, J. Marlet, A pig model of chronic hepatitis E displaying persistent viremia and a downregulation of innate immune responses in the liver. *Hepatol. Commun.* **7**, e0274 (2023).
17. S. U. Emerson, H. T. Nguyen, U. Torian, D. Burke, R. Engle, R. H. Purcell, Release of genotype 1 hepatitis E virus from cultured hepatoma and polarized intestinal cells depends on open reading frame 3 protein and requires an intact PXXP motif. *J. Virol.* **84**, 9059–9069 (2010).
18. J. Schuijers, J. P. Junker, M. Mokry, P. Hatzis, B. K. Koo, V. Sasselli, L. G. van der Flier, E. Cuppen, A. van Oudenaarden, H. Clevers, Ascl2 acts as an R-spondin/Wnt-responsive switch to control stemness in intestinal crypts. *Cell Stem Cell* **16**, 158–170 (2015).
19. A. S. Darwich, U. Aslam, D. M. Ashcroft, A. Rostami-Hodjegan, Meta-analysis of the turnover of intestinal epithelia in preclinical animal species and humans. *Drug Metab. Dispos.* **42**, 2016–2022 (2014).
20. L. G. van der Flier, H. Clevers, Stem cells, self-renewal, and differentiation in the intestinal epithelium. *Annu. Rev. Physiol.* **71**, 241–260 (2009).
21. J. R. Spence, C. N. Mayhew, S. A. Rankin, M. F. Kuhar, J. E. Vallance, K. Tolle, E. E. Hoskins, V. V. Kalinichenko, S. I. Wells, A. M. Zorn, N. F. Shroyer, J. M. Wells, Directed differentiation of human pluripotent stem cells into intestinal tissue in vitro. *Nature* **470**, 105–109 (2011).
22. N. Santos-Ferreira, X. Zhang, L. Corneillie, J. Van Dycke, W. Chiu, C. Montpellier, J. Neyts, L. Cocquerel, S. J. F. Kaptein, J. Rocha-Pereira, Proliferative cell targeting and epithelial cell turnover fuels hepatitis E virus replication in human intestinal enteroids. *Gastro Hep Adv.* **5**, 100769 (2026).
23. F. Liu, T. Liu, X. Wu, Z. Yu, J. Tong, L. Wang, C. Zhao, J. Nie, Y. Wang, K. Wang, L. Bai, P. Xia, K. Wang, G. Wei, Z. Z. Zheng, D. Wu, W. Huang, L. Wang, iPSC-induced multilineage liver organoids, small intestinal organoids and brain organoids sustain pangenotype hepatitis E virus propagation. *Gut*, 10.1136/gutjnl-2025-336105 (2025).
24. K. Liu, Y. Wang, J. Zhou, J. J. van der Meij, L. J. W. van der Laan, P. Li, Q. Pan, Decoding the role of the intestinal epithelium in hepatitis E virus infection using a human organoid prototype of "gut-liver" axis. *Virology* **610**, 110615 (2025).
25. A. Beer, H. Holzmann, S. Pischke, P. Behrendt, F. Wrba, J. Schlue, U. Drebber, B. Neudert, E. Halilbasic, H. Kreipe, A. Lohse, M. Sterneck, H. Wedemeyer, M. Manns, H. P. Dienes, Chronic hepatitis E is associated with cholangitis. *Liver Int.* **39**, 1876–1883 (2019).
26. B. Csernalabics, M. S. Marinescu, L. Maurer, L. Kelsch, J. Werner, K. Baumann, K. Zoldan, M. Panning, P. Reuken, T. Bruns, B. Bengsch, C. Neumann-Haefelin, M. Hofmann, R. Thimme, V. L. Dao Thi, T. Boettler, Efficient formation and maintenance of humoral and CD4 T-cell immunity targeting the viral capsid in acute-resolving hepatitis E infection. *J. Hepatol.* **80**, 564–575 (2024).
27. R. Fu, P. Jordan, Z. Engels, J. A. Weihs, J. Murle, H. Chi, S. Burbano de Lara, B. Helm, M. Klohn, J. Hu, A. Freistaedter, T. Boettler, M. Binder, U. Klingmuller, E. Steinmann, P. Y. Lozach, T. Tubiana, S. M. Lemon, V. L. Dao Thi, Integrin beta 1 facilitates non-enveloped hepatitis E virus cell entry through the recycling endosome. *Nat. Commun.* **16**, 5403 (2025).
28. M. Migueres, S. Lhomme, J. Izopet, Hepatitis A: Epidemiology, high-risk groups, prevention and research on antiviral treatment. *Viruses* **13**, 1900 (2021).
29. S. E. Blutt, O. D. Klein, M. Donowitz, N. Shroyer, C. Guha, M. K. Estes, Use of organoids to study regenerative responses to intestinal damage. *Am. J. Physiol. Gastrointest. Liver Physiol.* **317**, G845–G852 (2019).
30. M. Qu, L. Xiong, Y. Lyu, X. Zhang, J. Shen, J. Guan, P. Chai, Z. Lin, B. Nie, C. Li, J. Xu, H. Deng, Establishment of intestinal organoid cultures modeling injury-associated epithelial regeneration. *Cell Res.* **31**, 259–271 (2021).
31. G. Obert, I. Peiffer, A. L. Servin, Rotavirus-induced structural and functional alterations in tight junctions of polarized intestinal Caco-2 cell monolayers. *J. Virol.* **74**, 4645–4651 (2000).
32. C. A. Blank, D. A. Anderson, M. Beard, S. M. Lemon, Infection of polarized cultures of human intestinal epithelial cells with hepatitis A virus: Vectorial release of progeny virions through apical cellular membranes. *J. Virol.* **74**, 6476–6484 (2000).
33. A. Falkenhagen, J. Panajotov, R. Johne, Colon-derived Caco-2 cells support replication of hepatitis E virus genotype 1 strain Sar55 generated by reverse genetics. *Virus Res.* **347**, 199427 (2024).
34. J. W. Schoggins, S. J. Wilson, M. Panis, M. Y. Murphy, C. T. Jones, P. Bieniasz, C. M. Rice, A diverse range of gene products are effectors of the type I interferon antiviral response. *Nature* **472**, 481–485 (2011).
35. K. N. Bell, N. F. Shroyer, Krüpple-like factor 5 is required for proper maintenance of adult intestinal crypt cellular proliferation. *Dig. Dis. Sci.* **60**, 86–100 (2015).
36. O. Basak, M. van de Born, J. Korving, J. Beumer, S. van der Elst, J. H. van Es, H. Clevers, Mapping early fate determination in Lgr5$^+$ crypt stem cells using a novel *Ki67-RFP* allele. *EMBO J.* **33**, 2057–2068 (2014).
37. J. G. Kuruvilla, A. M. Ghaleb, A. B. Bialkowska, M. O. Nandan, V. W. Yang, Role of Krüppel-like factor 5 in the maintenance of the stem cell niche in the intestinal crypt. *Stem Cell Transl. Investig.* **2**, e839 (2015).
38. A. L. Haber, M. Biton, N. Rogel, R. H. Herbst, K. Shekhar, C. Smillie, G. Burgin, T. M. Delorey, M. R. Howitt, Y. Katz, I. Tirosh, S. Beyaz, D. Dionne, M. Zhang, R. Raychowdhury, W. S. Garrett, O. Rozenblatt-Rosen, H. N. Shi, O. Yilmaz, R. J. Xavier, A. Regev, A single-cell survey of the small intestinal epithelium. *Nature* **551**, 333–339 (2017).
39. V. L. D. Thi, Y. Debing, X. Wu, C. M. Rice, J. Neyts, D. Moradpour, J. Gouttenoire, Sofosbuvir inhibits hepatitis E virus replication in vitro and results in an additive effect when combined with ribavirin. *Gastroenterology* **150**, 82–85.e4 (2016).
40. W. Liu, G. P. Rodgers, Olfactomedin 4 is not a precise marker for human intestinal stem cells, but is involved in intestinal carcinogenesis. *Gastroenterology* **162**, 1001–1004 (2022).
41. J. Hu, T. Liu, M. Klöhn, A. Freistaedter, A. Toprak, H. Chi, P. Jordan, X. Yang, J. Becker, V. Lohmann, E. Steinmann, L. Wang, V. L. Dao Thi, The nucleotide analog bemnifosbuvir inhibits hepatitis E virus replication in preclinical models. bioRxiv 670060 [Preprint] (2025). https://doi.org/10.1101/2025.08.15.670060.
42. T. Lebedev, A. Mikheeva, V. Gasca, P. Spirin, V. Prassolov, Systematic comparison of FBS and medium variation effect on key cellular processes using morphological profiling. *Cells* **14**, 336 (2025).
43. M. K. Dame, S. Huang, D. Attili, J. R. Spence, J. A. Colacino, Identification and isolation of human LGR5$^+$ cells using an antibody-based strategy. *Methods Mol. Biol.* **2171**, 3–23 (2020).

Downloaded from https://www.science.org at Deutsches Krebsforschungszentrum on June 05, 2026

ERRATUM POSTED 15 MAY 2026; SEE LAST PAGE

44. H. Yan, Y. Ye, H. Zhao, H. Zuo, Y. Li, Single-cell RNA sequencing for analyzing the intestinal tract in healthy and diseased individuals. *Front. Cell Dev. Biol.* **10**, 915654 (2022).
45. P. Bastide, C. Darido, J. Pannequin, R. Kist, S. Robine, C. Marty-Double, F. Bibeau, G. Scherer, D. Joubert, F. Hollande, P. Blache, P. Jay, Sox9 regulates cell proliferation and is required for Paneth cell differentiation in the intestinal epithelium. *J. Cell Biol.* **178**, 635–648 (2007).
46. G. W. Webb, S. Kelly, H. R. Dalton, Hepatitis A and hepatitis E: Clinical and epidemiological features, diagnosis, treatment, and prevention. *Clin. Microbiol. Newsl.* **42**, 171–179 (2020).
47. A. Hirai-Yuki, L. Hensley, J. K. Whitmire, S. M. Lemon, Biliary secretion of quasi-enveloped human hepatitis A virus. *mBio* **7**, e01998-16 (2016).
48. G. M. Tjon, R. A. Coutinho, A. van den Hoek, S. Esman, C. J. Wijkmans, C. J. Hoebe, B. Wolters, C. Swaan, R. B. Geskus, N. Dukers, S. M. Bruisten, High and persistent excretion of hepatitis A virus in immunocompetent patients. *J. Med. Virol.* **78**, 1398–1405 (2006).
49. M. Takahashi, T. Tanaka, M. Azuma, E. Kusano, T. Aikawa, T. Shibayama, Y. Yazaki, H. Mizuo, J. Inoue, H. Okamoto, Prolonged fecal shedding of hepatitis E virus (HEV) during sporadic acute hepatitis E: Evaluation of infectivity of HEV in fecal specimens in a cell culture system. *J. Clin. Microbiol.* **45**, 3671–3679 (2007).
50. M. Zheng, Z. Tian, Liver-mediated adaptive immune tolerance. *Front. Immunol.* **10**, 2525 (2019).
51. S. Triana, C. Metz-Zumaran, C. Ramirez, C. Kee, P. Doldan, M. Shahraz, D. Schraivogel, A. R. Gschwind, A. K. Sharma, L. M. Steinmetz, C. Herrmann, T. Alexandrov, S. Boulant, M. L. Stanifer, Single-cell analyses reveal SARS-CoV-2 interference with intrinsic immune response in the human gut. *Mol. Syst. Biol.* **17**, e10232 (2021).
52. M. M. Lamers, J. Beumer, J. van der Vaart, K. Knoops, J. Puschhof, T. I. Breugem, R. B. G. Ravelli, J. Paul van Schayck, A. Z. Mykytyn, H. Q. Duimel, E. van Donselaar, S. Riesebosch, H. J. H. Kuijpers, D. Schipper, W. J. van de Wetering, M. de Graaf, M. Koopmans, E. Cuppen, P. J. Peters, B. L. Haagmans, H. Clevers, SARS-CoV-2 productively infects human gut enterocytes. *Science* **369**, 50–54 (2020).
53. J. T. Gebert, F. Scribano, K. A. Engevik, J. L. Perry, J. M. Hyser, Gastrointestinal organoids in the study of viral infections. *Am. J. Physiol. Gastrointest. Liver Physiol.* **324**, G51–G59 (2023).
54. A. K. Mehnert, S. Stegmaier, C. Ramirez Alvarez, E. Toprak, V. G. Magalhaes, C. Siebenkotten, J. Hu, A. L. Costa, D. Kirrmaier, M. Knop, X. Wu, T. Tubiana, C. Herrmann, M. Binder, V. L. Dao Thi, The hepatitis E virus capsid protein ORF2 counteracts cell-intrinsic antiviral responses to enable persistent replication in cell culture. *PLOS Pathog.* **21**, e1013516 (2025).
55. X. Wu, V. L. Dao Thi, Y. Huang, E. Billerbeck, D. Saha, H. H. Hoffmann, Y. Wang, L. A. V. Silva, S. Sarbanes, T. Sun, L. Andrus, Y. Yu, C. Quirk, M. Li, M. R. MacDonald, W. M. Schneider, X. An, B. R. Rosenberg, C. M. Rice, Intrinsic immunity shapes viral resistance of stem cells. *Cell* **172**, 423–438.e25 (2018).
56. S. A. Peters, C. R. Jones, A. L. Ungell, O. J. Hatley, Predicting drug extraction in the human gut wall: Assessing contributions from drug metabolizing enzymes and transporter proteins using preclinical models. *Clin. Pharmacokinet.* **55**, 673–696 (2016).
57. S. T. Susa, A. Hussain, C. V. Preuss, "Drug metabolism," in *StatPearls* [Treasure Island (FL), 2025].
58. D. Babusis, M. P. Curry, B. Kirby, Y. Park, E. Murakami, T. Wang, A. Mathias, N. Afdhal, J. G. McHutchison, A. S. Ray, Sofosbuvir and ribavirin liver pharmacokinetics in patients infected with hepatitis C virus. *Antimicrob. Agents Chemother.* **62**, e02587-17 (2018).
59. T. Wang, D. Babusis, Y. Park, C. Niu, C. Kim, X. Zhao, B. Lu, B. Ma, R. C. Muench, D. Sperger, A. S. Ray, E. Murakami, Species differences in liver accumulation and metabolism of nucleotide prodrug sofosbuvir. *Drug Metab. Pharmacokinet.* **35**, 334–340 (2020).
60. K. Mori, O. Hiraoka, M. Ikeda, Y. Ariumi, A. Hiramoto, Y. Wataya, N. Kato, Adenosine kinase is a key determinant for the anti-HCV activity of ribavirin. *Hepatology* **58**, 1236–1244 (2013).
61. M. Uhlén, L. Fagerberg, B. M. Hallstrom, C. Lindskog, P. Oksvold, A. Mardinoglu, A. Sivertsson, C. Kampf, E. Sjöstedt, A. Asplund, I. Olsson, K. Edlund, E. Lundberg, S. Navani, C. A. Szigyarto, J. Odeberg, D. Djureinovic, J. O. Takanen, S. Hober, T. Alm, P. H. Edqvist, H. Berling, H. Tegel, J. Mulder, J. Rockberg, P. Nilsson, J. M. Schwenk, M. Hamsten, K. von Feilitzen, M. Forsberg, L. Persson, F. Johansson, M. Zwahlen, G. von Heijne, J. Nielsen, F. Pontén, Proteomics. Tissue-based map of the human proteome. *Science* **347**, 1260419 (2015).
62. J. Burclaff, R. J. Bliton, K. A. Breau, M. T. Ok, I. Gomez-Martinez, J. S. Ranek, A. P. Bhatt, J. E. Purvis, J. T. Woosley, S. T. Magness, A proximal-to-distal survey of healthy adult human small intestine and colon epithelium by single-cell transcriptomics. *Cell. Mol. Gastroenterol. Hepatol.* **13**, 1554–1589 (2022).
63. N. Kamar, F. Abravanel, P. Behrendt, J. Hofmann, G. P. Pageaux, C. Barbet, V. Moal, L. Couzi, T. Horvatits, R. A. De Man, E. Cassuto, A. M. Elsharkawy, A. Riezebos-Brilman, A. Scemla, S. Hillaire, M. C. Donnelly, S. Radenne, J. Sayegh, C. Garrouste, J. Dumortier, F. Glowaki, M. Matignon, A. Coilly, L. Figueres, C. Mousson, A. Minello, S. Dharancy, J. P. Rerolle, P. Lebray, I. Etienne, P. Perrin, M. Choi, O. Marion, J. Izopet, Hepatitis E Virus Ribavirin Study Group, Ribavirin for hepatitis E virus infection after organ transplantation: A large European retrospective multicenter study. *Clin. Infect. Dis.* **71**, 1204–1211 (2020).
64. M. Crespo, E. Vilar, S. Y. Tsai, K. Chang, S. Amin, T. Srinivasan, T. Zhang, N. H. Pipalia, H. J. Chen, M. Witherspoon, M. Gordillo, J. Z. Xiang, F. R. Maxfield, S. Lipkin, T. Evans, S. Chen, Colonic organoids derived from human induced pluripotent stem cells for modeling colorectal cancer and drug testing. *Nat. Med.* **23**, 878–884 (2017).
65. S. Yoshida, H. Miwa, T. Kawachi, S. Kume, K. Takahashi, Generation of intestinal organoids derived from human pluripotent stem cells for drug testing. *Sci. Rep.* **10**, 5989 (2020).
66. M. S. Hakim, S. Chen, S. Ding, Y. Yin, A. Ikram, X. X. Ma, W. Wang, M. P. Peppelenbosch, Q. Pan, Basal interferon signaling and therapeutic use of interferons in controlling rotavirus infection in human intestinal cells and organoids. *Sci. Rep.* **8**, 8341 (2018).
67. F. Masmoudi, N. Santos-Ferreira, D. Pajkrt, K. C. Wolthers, J. DeGroot, M. L. H. Vlaming, J. Rocha-Pereira, L. Buti, Evaluation of 3D human intestinal organoids as a platform for EV-A71 antiviral drug discovery. *Cells* **12**, 1138 (2023).
68. C. Zhang, A. Freistaedter, C. Schmelas, M. Gunkel, V. L. Dao Thi, D. Grimm, An RNA iterference/adeno-associated virus vector-based combinatorial gene therapy approach against hepatitis E virus. *Hepatol. Commun.* **6**, 878–888 (2022).
69. D. Aran, A. P. Looney, L. Liu, E. Wu, V. Fong, A. Hsu, S. Chak, R. P. Naikawadi, P. J. Wolters, A. R. Abate, A. J. Butte, M. Bhattacharya, Reference-based analysis of lung single-cell sequencing reveals a transitional profibrotic macrophage. *Nat. Immunol.* **20**, 163–172 (2019).
70. M. Kang, J. J. A. Armenteros, G. S. Gulati, R. Gleyzer, S. Avagyan, E. L. Brown, W. Zhang, A. Usmani, N. Earland, Z. Wu, J. Zou, R. C. Fields, D. Y. Chen, A. A. Chaudhuri, A. M. Newman, Mapping single-cell developmental potential in health and disease with interpretable deep learning. bioRxiv 585637 [Preprint] (2024). https://doi.org/10.1101/2024.03.19.585637.
71. J. Cao, M. Spielmann, X. Qiu, X. Huang, D. M. Ibrahim, A. J. Hill, F. Zhang, S. Mundlos, L. Christiansen, F. J. Steemers, C. Trapnell, J. Shendure, The single-cell transcriptional landscape of mammalian organogenesis. *Nature* **566**, 496–502 (2019).
72. A. Butler, P. Hoffman, P. Smibert, E. Papalexi, R. Satija, Integrating single-cell transcriptomic data across different conditions, technologies, and species. *Nat. Biotechnol.* **36**, 411–420 (2018).
73. M. Milacic, D. Beavers, P. Conley, C. Gong, M. Gillespie, J. Griss, R. Haw, B. Jassal, L. Matthews, B. May, R. Petryszak, E. Ragueneau, K. Rothfels, C. Sevilla, V. Shamovsky, R. Stephan, K. Tiwari, T. Varusai, J. Weiser, A. Wright, G. Wu, L. Stein, H. Hermjakob, P. D'Eustachio, The Reactome Pathway Knowledgebase 2024. *Nucleic Acids Res.* **52**, D672–D678 (2024).
74. G. W. He, L. Lin, J. DeMartino, X. Zheng, N. Staliarova, T. Dayton, H. Begthel, W. J. van de Wetering, E. Bodewes, J. van Zon, S. Tans, C. Lopez-Iglesias, P. J. Peters, W. Wu, D. Kotlarz, C. Klein, T. Margaritis, F. Holstege, H. Clevers, Optimized human intestinal organoid model reveals interleukin-22-dependency of paneth cell formation. *Cell Stem Cell* **29**, 1333–1345.e6 (2022).
75. H. Miyoshi, T. S. Stappenbeck, In vitro expansion and genetic modification of gastrointestinal stem cells in spheroid culture. *Nat. Protoc.* **8**, 2471–2482 (2013).
76. M. Fujii, M. Matano, K. Toshimitsu, A. Takano, Y. Mikami, S. Nishikori, S. Sugimoto, T. Sato, Human intestinal organoids maintain self-renewal capacity and cellular diversity in niche-inspired culture condition. *Cell Stem Cell* **23**, 787–793.e6 (2018).
77. H.-E. Huang, O. Colasanti, T. F. Li, V. Lohmann, Limited impact of hepatitis A virus 3C protease-mediated cleavage on the functions of NEMO in human hepatocytes. *J. Virol.* **99**, e0226424 (2025).
78. F. Sampaziotis, D. Muraro, O. C. Tysoe, S. Sawiak, T. E. Beach, E. M. Godfrey, S. S. Upponi, T. Brevini, B. T. Wesley, J. Garcia-Bernardo, K. Mahbubani, G. Canu, R. Gieseck III, N. L. Berntsen, V. L. Mulcahy, K. Crick, C. Fear, S. Robinson, L. Swift, L. Gambardella, J. Bargehr, D. Ortmann, S. E. Brown, A. Osnato, M. P. Murphy, G. Corbett, W. T. H. Gelson, G. F. Mells, P. Humphreys, S. E. Davies, I. Amin, P. Gibbs, S. Sinha, S. A. Teichmann, A. J. Butler, T. C. See, E. Melum, C. J. E. Watson, K. Saeb-Parsy, L. Vallier, Cholangiocyte organoids can repair bile ducts after transplantation in the human liver. *Science* **371**, 839–846 (2021).
79. M. Huch, H. Gehart, R. van Boxtel, K. Hamer, F. Blokzijl, M. M. Verstegen, E. Ellis, M. van Wenum, S. A. Fuchs, J. de Ligt, M. van de Wetering, N. Sasaki, S. J. Boers, H. Kemperman, J. de Jonge, J. N. Ijzermans, E. E. Nieuwenhuis, R. Hoekstra, S. Strom, R. R. Vries, L. J. van der Laan, E. Cuppen, H. Clevers, Long-term culture of genome-stable bipotent stem cells from adult human liver. *Cell* **160**, 299–312 (2015).
80. J. Zhao, P. Shu, F. Duan, X. Wang, L. Min, Z. Shen, Y. Ruan, J. Qin, Y. Sun, X. Qin, Loss of OLFM4 promotes tumor migration through inducing interleukin-8 expression and predicts lymph node metastasis in early gastric cancer. *Oncogenesis* **5**, e234 (2016).
81. X. Kong, X. Chen, S. Ou, W. Wang, R. Li, Derivation of human triploid trophoblast stem cells. *J. Assist. Reprod. Genet.* **39**, 1183–1193 (2022).
82. H. Gorman, F. Moreau, A. Dufour, K. Chadee, IgGFc-binding protein and MUC2 mucin produced by colonic goblet-like cells spatially interact non-covalently and regulate wound healing. *Front. Immunol.* **14**, 1211336 (2023).
83. J. Beumer, J. Puschhof, F. Y. Yengej, L. Zhao, A. Martinez-Silgado, M. Blotenburg, H. Begthel, C. Boot, A. van Oudenaarden, Y. G. Chen, H. Clevers, BMP gradient along the intestinal villus axis controls zonated enterocyte and goblet cell states. *Cell Rep.* **38**, 110438 (2022).

Downloaded from https://www.science.org at Deutsches Krebsforschungszentrum on June 05, 2026

ERRATUM POSTED 15 MAY 2026; SEE LAST PAGE

84. B. Wang, Y. Zhu, C. Yu, C. Zhang, Q. Tang, H. Huang, Z. Zhao, Hepatitis C virus induces oxidation and degradation of apolipoprotein B to enhance lipid accumulation and promote viral production. *PLOS Pathog.* **17**, e1009889 (2021).

Acknowledgments: We thank S. Emerson, R. Ulrich, H. G. Kräusslich, and S. Duncan for sharing reagents. We acknowledge S. Jones and the Center for Synthetic Genomics for support with writing the manuscript and preparation of the figures. For the publication fee, we acknowledge financial support by Heidelberg University and TRR179. We also acknowledge the data storage service SDS@hd, supported by the Ministry of Science, Research and the Arts Baden-Württemberg (MWK) and by the German Research Foundation (DFG) through grant INST 35/1314-1 FUGG and INST 35/1503-1 FUGG. We acknowledge the CMCP and wissenschaftlich-histologisches Labor, Pathologisches Institut, for processing the organoid samples. We acknowledge microscopy support from the Infectious Diseases Imaging Platform (IDIP) at the Center for Integrative Infectious Disease Research Heidelberg and V. Weinhardt for sharing SPIM expertise. We are grateful for the support of A.-K. Mehnert, D. Ibberson, and the Deep Sequencing Core Facility. We thank U. Merle for the collection of stool samples from HAV patients. We are grateful to the members of Child Health Research Foundation and Popular Diagnostic Center Limited (H. Rahman, Md. S. Kabir, A. Malaker, S. Debnath, A. M. Tanmoy, M. Haque, P. Mondal, and Md. A. Rahman) for the assistance with patient identification, patient follow-up, and sample collection. We thank J. Puschhof for valuable and helpful discussions and N. Cetin (STEMCELL Technologies) for excellent scientific input. We are also grateful to A. Freistaedter and J. Becker for outstanding technical assistance. **Funding:** This work was supported by the Deutsche Forschungsgemeinschaft (DFG; German Research Foundation), Projektnummer 272983813 TP11, TP04, TP17, and TP22 TRR 179 (S.P., H.-E.H., C.B., T.B., V.L., and V.L.D.T.); the Chica and Heinz Schaller Foundation and German Center for Infection Research (DZIF), TTU Hepatitis Project 05.823 (V.L.D.T.); the Forschungsprogramm "Antivirale Therapien" from Baden-Württemberg Stiftung (S.P., V.Lo., and V.L.D.T.); China Scholarship Council (J.H.); the Structured Doctoral Programme (Strukturiertes Doktorandenprogramm zum Erwerb des Dr. med. und Dr. rer. nat.) of Heidelberg University (C.A.); the German Center for Infection Research (DZIF) (C.B.); the Deutsche Forschungsgemeinschaft (DFG; German Research Foundation) under Germany's Excellence Strategy via the Excellence Cluster 3D Matter Made to Order (EXC-2082/1-390761711) (J.W.); and the Max Eder grant by the German Cancer Aid (no. 70113858) (M.T.D.). **Author contributions:** Conceptualization: S.P., M.T.D., and V.L.D.T. Methodology: S.P., A.L., S.S., J.W., C.H., M.T.D., and V.L.D.T. Investigation: S.P., N.M., C.A., A.L., H.-E.H., J.H., E.T., D.P.K., O.C., and N.L.-J. Visualization: S.P., N.M., C.A., A.L., H.-E.H., J.H., C.H., and V.L.D.T. Resource: J.M., C.B., C.M., P.P., P.B., T.B., E.S., S.S., V.Lo., and M.T.D. Software: S.P., N.M., C.A., A.L., J.H., V.La., and C.H. Supervision: V.L.D.T. Writing—original draft: S.P., N.M., C.A., A.L., and V.L.D.T. Writing—review and editing: S.P., A.L., and V.L.D.T. **Competing interests:** The authors declare that they have no competing interests. **Data, code, and materials availability:** All data and code needed to evaluate and reproduce the results in the paper are present in the paper and/or the Supplementary Materials. Custom code used for analysis is available at https://zenodo.org/records/18782623. This study did not generate new materials. The scRNA-seq data have been deposited in NCBI's Gene Expression Omnibus and are accessible through GEO Series accession no. GSE303209. The human intestinal organoid materials can be provided by M.T.D.'s pending scientific review and a completed material transfer agreement with Heidelberg University Hospital. Requests for human intestinal organoid lines should be submitted to michael.dill@med.uni-heidelberg.de.

Submitted 5 August 2025
Accepted 26 February 2026
Published 1 April 2026
10.1126/sciadv.aeb2333

Downloaded from https://www.science.org at Deutsches Krebsforschungszentrum on June 05, 2026

Erratum

Post date 15 May 2026

Erratum for the Research Article "Hepatitis E virus replication is maintained in proliferative cells within the intestinal crypt" by S. Prallet *et al*.

The original version of the Research Article, "Hepatitis E virus replication is maintained in proliferative cells within the intestinal crypt" by S. Prallet *et al*. contained an error in Fig. 5.

The following corrections have been implemented:

- During the preparation of Fig. 5, the representative image for ORF2/Nuclei at 48 hours inadvertently duplicated the image for 99 hours in panel A. Figure 5 has been updated to include the correct representative image for 48 hours.
- In the Fig. 5 caption, "Cycle Treshold" has been corrected to "Cycle Threshold."

Figure 5 has been corrected in the PDF and HTML versions of the article.

Downloaded from https://www.science.org at Deutsches Krebsforschungszentrum on June 05, 2026

10.1126/sciadv. aei2438

ScienceAdvances

Hepatitis E virus replication is maintained in proliferative cells within the intestinal crypt

Sarah Prallet, Niclas Maier, Albert Li, Cassian Afting, Hao-En Huang, Jungen Hu, Elif Toprak, Deb Purna Keya, Ombretta Colasanti, Nancy León-Janampa, Julien Marlet, Claudia Beisel, Carolin Mogler, Philip Puchas, Patrick Behrendt, Tobias Boettler, Eike Steinmann, Senjuti Saha, Vibor Laketa, Volker Lohmann, Joachim Wittbrodt, Carl Hermann, Michael T. Dill, and Viet Loan Dao Thi

Sci. Adv. **12** (14), eaeb2333. DOI: 10.1126/sciadv.aeb2333

View the article online
https://www.science.org/doi/10.1126/sciadv.aeb2333
Permissions
https://www.science.org/help/reprints-and-permissions

Downloaded from https://www.science.org at Deutsches Krebsforschungszentrum on June 05, 2026

Use of this article is subject to the Terms of service

Science Advances (ISSN 2375-2548) is published by the American Association for the Advancement of Science. 1200 New York Avenue NW, Washington, DC 20005. The title *Science Advances* is a registered trademark of AAAS.

Copyright © 2026 The Authors, some rights reserved; exclusive licensee American Association for the Advancement of Science. No claim to original U.S. Government Works. Distributed under a Creative Commons Attribution NonCommercial License 4.0 (CC BY-NC).